

FRET as the tool for in vivo nanomedicine tracking

Norraseth Kaeokhamloed, Samuel Legeay, Emilie Roger

▶ **To cite this version:**

Norraseth Kaeokhamloed, Samuel Legeay, Emilie Roger. FRET as the tool for in vivo nanomedicine tracking. Journal of Controlled Release, 2022, 349, pp.156-173. 10.1016/j.jconrel.2022.06.048 . hal-03720790

HAL Id: hal-03720790

https://univ-angers.hal.science/hal-03720790

Submitted on 12 Jul 2022

HAL is a multi-disciplinary open access archive for the deposit and dissemination of scientific research documents, whether they are published or not. The documents may come from teaching and research institutions in France or abroad, or from public or private research centers.

L'archive ouverte pluridisciplinaire **HAL**, est destinée au dépôt et à la diffusion de documents scientifiques de niveau recherche, publiés ou non, émanant des établissements d'enseignement et de recherche français ou étrangers, des laboratoires publics ou privés.



Distributed under a Creative Commons Attribution - NonCommercial - NoDerivatives 4.0 International License

Journal of Controlled Release 349 (2022) 156–173

Contents lists available at ScienceDirect

Journal of Controlled Release

journal homepage: www.elsevier.com/locate/jconrel

Review article

FRET as the tool for *in vivo* nanomedicine tracking

Norraseth Kaeokhamloed, Samuel Legeay, Emilie Roger *

MINT, INSERM U1066, CNRS 6021, SFR-ICAT, University of Angers, 49333 Angers, France

ARTICLE INFO

Keywords:
FRET
Pharmacokinetics
Nanomedicine
In vivo fluorescence imaging
Confocal microscopy

ABSTRACT

Advanced drug delivery system utilizing a nanocarrier is the major application of nanotechnology on pharmacotherapeutics. However, despite the promising benefits and a leading trend in pharmaceutical research, nanomedicine development suffers from a poor clinical translation problem as only a handful of nanomedicine products reach the market yearly. The conventional pharmacokinetic study generally focuses only on monitoring the level of a free drug but ignores the nanocarrier's role in pharmacokinetics. One hurdle is that it is difficult to directly track intact nanocarriers *in vivo* to explore their pharmacokinetics. Although several imaging techniques such as radiolabeling, nuclear imaging, fluorescence imaging, *etc.*, have been developed over the past few years, currently, one method that can successfully track the intact nanocarriers *in vivo* directly is by *Förster resonance energy transfer* (FRET). This review summarizes the application of FRET as the *in vivo* nanoparticle tracker for studying the *in vivo* pharmacokinetics of the organic nanocarriers and gives elaborative details on the techniques utilized.

1. Introduction

The European Medicine Agency (EMA) defines 'nanomedicine' as the application of nanotechnology aiming for clinical diagnosis and therapeutic use [1]. Advanced drug delivery system utilizing a nanocarrier is the major application of nanotechnology on pharmacotherapeutics [2]. The main benefits of the nanocarrier delivery system include targeted drug delivery, reducing side effects, enhancing bioavailability, and controlling drug release. With the versatility to carry either large or small molecule drugs, biologics, and genetic materials, the nanocarrier delivery system provides a viable solution for the delivery problem encountered in conventional drug formulation [1–3]. However, despite the promising benefits and a leading trend in pharmaceutical research, nanomedicine development suffers from a poor clinical translation problem as only a handful of nanomedicine products reach the market yearly [4,5]. The lack of a complete understanding of nanomedicine's pharmacokinetics contributes to the cause of this failure. The conventional pharmacokinetic study generally focuses only on monitoring drug levels but ignores the nanocarrier's role in pharmacokinetics. This approach is certainly inadequate for the overall understanding of a drug's pharmacokinetics because the interaction that a body acts upon a nanocarrier also directly affects the pharmacokinetics, the therapeutic efficacy, and the safety of the loading drug [6,7]. Moreover, there are many more aspects of pharmacokinetics in the context of nanomedicine, for example, particle integrity, drug release, particle internalization, *etc.*, which are difficult to be explained using the classical ADME (absorption, distribution, metabolism, and elimination) model alone. Therefore, to obtain a complete view of the pharmacokinetics of the nanomedicine, the pharmacokinetics of the intact nanocarriers is as important and needs to be investigated [8,9].

Up until now, the advanced pharmacokinetic analysis on the nanocarriers is still limited, especially for the organic nanomedicine [8,9]: lipid-based and polymer-based nanoparticles [3]. Despite making up the largest group of nanomedicine in the market [10], the organic nanoparticles are difficult to be directly characterized *in vivo*, in tissue, and in biological fluid. Several imaging techniques have been developed over the past few years, trying to directly characterize the nanocarriers *in vivo*. Nuclear imaging using the radiolabel is one of the conventional techniques with high sensitivity for monitoring biodistribution and elimination. It can indirectly give quantitative information about the nanocarriers. However, radiolabeling needs to be strongly conjugated to the nanocarrier's structure, risking modifying the nanocarrier's physicochemical properties. The technique also gives a poor resolution and involves radioactive materials. Other imaging techniques such as computed tomography (CT) and magnetic resonance imaging (MRI) are also employed with the advantage of a higher resolution for organic nanoparticles. However, their operation cost is high, and those methods are not appropriate for organic nanoparticles detection. Thus, a simpler

* Corresponding author.
E-mail address: emilie.roger@univ-angers.fr (E. Roger).

https://doi.org/10.1016/j.jconrel.2022.06.048
Received 25 April 2022; Received in revised form 20 June 2022; Accepted 25 June 2022
0168-3659/© 2022 The Authors. Published by Elsevier B.V. This is an open access article under the CC BY-NC-ND license (http://creativecommons.org/licenses/by-nc-nd/4.0/).

and less expensive technique such as the fluorescence method is preferably used [9,11], particularly with the emergence of carbocyanine fluorescence dyes. The commercialized carbocyanine dyes have emission spectra covering the near-infrared (NIR) range (650–900 nm) which is the sweet spot for the *in vivo* fluorescence imaging due to less interference from the *in vivo* environment. This greatly improves fluorescence's specificity and tissue penetration. The dyes are biocompatible and can be encapsulated into the nanocarriers, rendering them ideal for tracing organic nanocarriers [12]. However, whole-body fluorescence imaging still gives a relatively low resolution, but this can be compensated by using the confocal fluorescence microscopy (CFM) technique in parallel. The technique acts as a fluorescence magnifying glass zooming into a small area of interest. It gives a very high resolution but loses the tissue penetration capability so that it is more suitable for imaging *ex vivo* tissue or organs [9,13].

Nevertheless, all of the techniques mentioned earlier have the same crucial problem that they cannot directly determine the particle integrity of organic nanoparticles. Currently, the only method that can characterize the particle integrity of organic nanoparticles is by *Förster resonance energy transfer* (FRET) [9,14,15]. It is a subset of the fluorescence technique often dubbed the 'nano-ruler' since the technique is very sensitive to the distance change in nanoscale and is thus proved to be useful for monitoring the association or the dissociation of organic nanoparticles [16]. Another advantage of FRET is that the commonly used carbocyanine dyes can be utilized, making it easier for the existing fluorescence imaging techniques to be upgraded to FRET [16,17]. Therefore, it is obvious that FRET can be an ideal tool for studying the pharmacokinetics of nanomedicine in the future. This review summarizes the application of FRET as the *in vivo* nanoparticle tracker for studying the *in vivo* pharmacokinetics of the organic nanocarriers and gives elaborative details on the techniques utilized.

2. General overview on FRET

Förster resonance energy transfer (FRET), a.k.a. the fluorescence resonance energy transfer, was discovered by Theodor Förster. [18,19] FRET is a non-radiative near-field resonance phenomenon originating from the dipole-dipole interaction between two fluorophore molecules, which can only occur at a very close distance (<10 nm). When one fluorophore is excited and in close proximity with another fluorophore whose absorption spectrum overlaps the first fluorophore's emission spectrum, the energy can be transferred from the first fluorophore to the second one (Fig. 1). The fluorophore that transfers the energy is called the donor, and the one receiving the energy is called the acceptor. The amount of energy absorbed by the donor that is transferred to the acceptor is the FRET efficiency (E_{FRET}), which is highly dependent on the distance (r) between the donor and acceptor by the factor of r^{-6}. FRET transfer rate is in equilibrium with the decay rate at $E_{FRET} = 50\%$, and as such, the corresponding r distance is defined as R_0 (Fig. 2). Thus, the E_{FRET} can be defined by the relationship with R_0 and r as the equation below [16,20,21].

$$E_{FRET} = \frac{R_0^6}{R_0^6 + r^6}$$

There are several ways to measure E_{FRET} based on the quantum yield, the fluorescence intensity, or the fluorescence lifetime, of which their details can be found elsewhere [20,22]. Herein, only the most commonly used techniques of FRET measurement are explained.

2.1. FRET proximity-based measurement

Proximity-based FRET measurement focuses on measuring E_{FRET} relating to the distance between the donor-acceptor (r). The E_{FRET} rapidly increases to 98% at the distance of $0.5R_0$ and conversely plummets to 1% at $2R_0$ (Fig. 2). Therefore, the distance range between $0.5R_0$ and $2R_0$ is very useful for the proximity measurement [16,23]. However, directly measuring E_{FRET} and R_0 is a complex task. Therefore, for practicality, E_{FRET} is simplified by correlating to the donor and acceptor intensity, giving a practical parameter called FRET proximity ratio (PR) as shown in the equation:

$$PR = \frac{I_{AD}}{(I_{AD} + I_{DA})}$$

Where I_{AD} and I_{DA} are the emission intensity of the FRET acceptor and the donor, respectively [24–28]. Sometimes, E_{FRET} is simplified to FRET intensity ratio, which is seldomly found in the literature [29,30].

$$Ratio = \frac{I_{AD}}{I_{DA}}$$

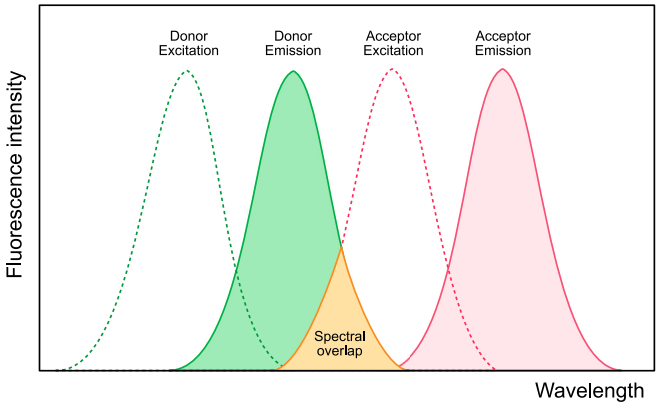


Fig. 1. FRET occurs when the donor emission spectrum overlaps the acceptor excitation spectrum (yellow area). (For interpretation of the references to colour in this figure legend, the reader is referred to the web version of this article.)

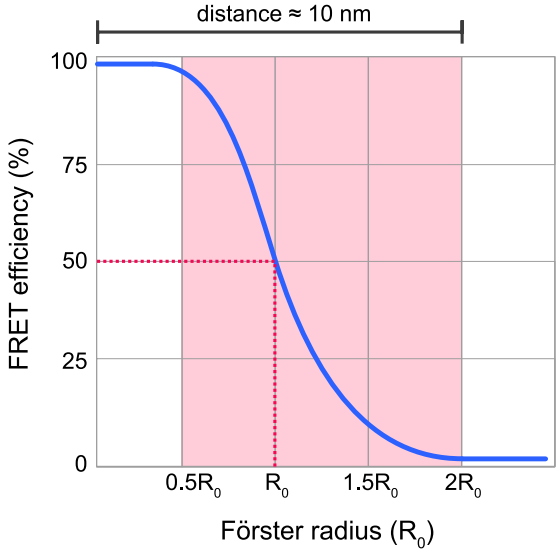


Fig. 2. Relationship between FRET efficiency (E_{FRET}) and Förster radius (R_0). FRET transfer rate is in equilibrium with the decay rate at $E_{FRET} = 50\%$, and as such, the corresponding donor-acceptor distance (r) is defined as R_0 (red dash line). E_{FRET} is highly dependent on r as it rapidly increases to 98% at the distance of $0.5R_0$ and conversely plummets to 1% at $2R_0$. Therefore, the distance range between $0.5R_0$ and $2R_0$ (red shading) is very useful for the proximity measurement. Generally, the distance of $2R_0$ is approximately 10 nm, which is why FRET occurs only at a nanoscale. Adapted from [23]. Copyright 2014, with permission from John Wiley and Sons. (For interpretation of the references to colour in this figure legend, the reader is referred to the web version of this article.)

Proximity-based FRET has the main application for monitoring the structural and conformational change of macromolecules at a molecular level. It can be used as a biosensor for either qualitative analysis for the spatial interaction as the on/off switch (FRET *vs.* No-FRET situations) or quantitative analysis as a nanoscale ruler [21,22,31].

2.2. FRET lifetime-based measurement

Fluorescence lifetime (τ) is the time interval that the fluorophore stays at the excited state before radiating the photon. Generally, it is around 10^{-9} s and follows the exponential decay as in the equation:

$$\frac{F(t)}{F(0)} = e^{-t/\tau}$$

Where *F(t)* is the photon count at the time *t*. Thus, the lifetime τ is defined as $F(0)/e \approx 37\%$ of the initial photon count [32,33]. For FRET application, the donor will transfer the energy to the acceptor *via* a non-radiating process resulting in the donor emission quenching and a decrease in τ. Thereby, E_{FRET} can be monitored from donor quenching as in the equation:

$$E_{FRET} = 1 - \left(\frac{\tau_{DA}}{\tau_D}\right) = 1 - \left(\frac{I_{DA}}{I_D}\right)$$

Where τ_{DA} is the donor lifetime with FRET, w_D is the donor lifetime without FRET, and likewise for the donor intensity (*I*) [20,22,33]. This FRET donor quenching technique is useful for dynamic fluorescence measurement, such as live-cell image analysis. The technique referred to as FRET Fluorescence lifetime imaging (FRET-FILM) is the combination of lifetime measurement and cellular imaging with FRET donor quenching. Indeed, the use of FRET helps to discriminate the endogenous molecules against the autofluorescence. FRET-FILM allows for live monitoring of several dynamic interactions such as receptor-ligand binding, protease activity, protein folding, hybridization of genetic materials [33].

3. FRET-nanomedicine applied to *in vivo* nanoparticles tracking

Generally, FRET proximity-based measurement is applied to nanomedicine to monitor the nanoparticle's structural change, including particle association, particle integrity, cargo release, and particle interaction with cells [15]. In the context of the pharmacokinetics of nanomedicine, especially the organic nanoparticles, FRET is usefully employed as the *in vivo* nanoparticle tracking technique because it is the technique that can determine nanoparticle's integrity both *in vivo* and *in vitro* [9]. Particle integrity is crucial for the pharmacokinetics of nanoparticles because the integrity defines the existence of the nanoparticle and the clinical benefits thereof, such as the protective effect to the encapsulated drugs, the organ targeting effect, the extravasation and membrane transport effect, *etc.* [1,2]. An ability to determine the intact nanoparticles *in vivo* will help to elucidate the *in vivo* pharmacokinetics of the nanocarriers, which is essential for clinical translation [4–7].

In vivo nanoparticle tracking requires a pair of FRET dyes (often called a FRET pair) to be integrated into the nanoparticle's structure rendering the FRET-nanoparticles. The FRET dyes of choice are the carbocyanine dyes with the emission spectra in the near-infrared (NIR) range (650–900 nm) to obtain high tissue penetration by avoiding autofluorescence from cells and tissues [12]. These dyes include, for example, non-sulfonated cyanines: Cy3, Cy5, Cy5.5, Cy7, Cy7.5, indocyanine green (ICG); and dialkylcarbocyanines (Di): DiO, DiR, DiI, DiD (Fig. 3) [34].

Despite following the same FRET principle, techniques to integrate the FRET dyes to make the system of FRET-nanoparticles vary by the structural and chemical differences of each type of the organic nanoparticles.

3.1. Polymeric micelles

Polymeric micelles are one of the most diverse groups in terms of chemical composition. However, they do share structural similarities. They have a property of self-assembling and structurally consist of the hydrophobic moiety (not entirely hydrophobic but less hydrophilic than the other part) resembling a core and the hydrophilic moiety resembling an outer shell. Carbocyanine dyes are mainly used as a FRET pair in this type of nanoparticle, and they can either be loaded into the hydrophobic core or be conjugated to the polymer itself, in order to reflect or mimic how drugs can actually be loaded to the nanocarrier. Therefore, it can be classified into a group of dye-loading FRET system and dye-conjugating FRET system (Fig. 4). In the dye-loading FRET system, carbocyanine dyes can be loaded into the hydrophobic core of the micelles. Besides, in the dye-conjugating FRET system, hydrophobic fluorescence dyes could be conjugated to the hydrophobic moiety of the polymer. Donor and acceptor FRET dyes are conjugated separately and then mixed together while forming a micelle consisting of a FRET pair. So, when the micelles dissociate, the conjugated-FRET pair will disperse out, resulting in the disappearance of the FRET signal. These different FRET systems imply different aspects of micelles stability and pharmacokinetics. The dye-loading FRET system implies cargo release. The dye-conjugating FRET system implies the dissociation of the micelles. This is useful for monitoring the pharmacokinetics of drugs loaded inside the micelle core. However, in terms of pharmacokinetic study of nanomedicine, those aspects are not practically different since the focus is on the nanoparticles' integrity rather than the loaded drugs.

3.2. Lipid nanocapsules and liposomes

Nanocapsules are a class of nanoparticles that contains a shell-like structure and a core resembling a capsule or a vesicle. Lipid nanocapsules and lipid nanoemulsions contain a monolayer shell of surfactant surrounding a lipid core. Liposomes are a vesicle with phospholipid bilayer shell. Carbocyanine dyes are utilized in this type of nanoparticles by the co-encapsulation inside the nanoparticle's core or void. All the FRET systems of lipid nanocapsules and liposomes are summarized in Fig. 5.

3.3. Nanospheres

Nanospheres are a class of nanoparticles that has a matrix structure. It is called nanospheres, although it does not need to be spherical in shape. It can be made of various organic and inorganic materials. However, FRET was only utilized in organic lipid or polymeric nanospheres for studying their *in vivo* pharmacokinetics. Nanospheres seem to be uniquely developed for delivering a specific drug. All three types of nanospheres have different strategies to incorporate FRET pairs. For the squalene-gemcitabine bioconjugate nanoparticles (SQGem nanospheres) [38], the FRET pair was conjugating to the matrix structure. For the c(CRGDKGPDC) peptide (iRGD) modified hyaluronic acid–deoxycholic acid conjugate (iRGD-PEG-HA-DOCA) a.k.a. IPHD nanoparticles [49], the FRET pair was simply dispersed in the polymer matrix. On the other hand, for the polymeric γPGA-EGTA nanoparticles [50,51], the FRET system is firstly conjugated to insulin before being loaded into the polymer matrix. The study also focused on the stability of the insulin in the GI tracts rather than the stability of the polymer matrix [50]. Fig. 6 summarizes all the FRET systems of nanospheres.

3.4. Nanocrystals

Nanocrystal is a crystal in the nanometer range formulated by nanoprecipitation of poorly water-soluble organic substances. There are two nanocrystals with FRET described: coumarin-6 nanocrystals [52] and curcumin nanocrystals (Fig. 7) [53]. While coumarin-6 nanocrystal can be paired with DiI to create a FRET system, curcumin nanocrystal loses

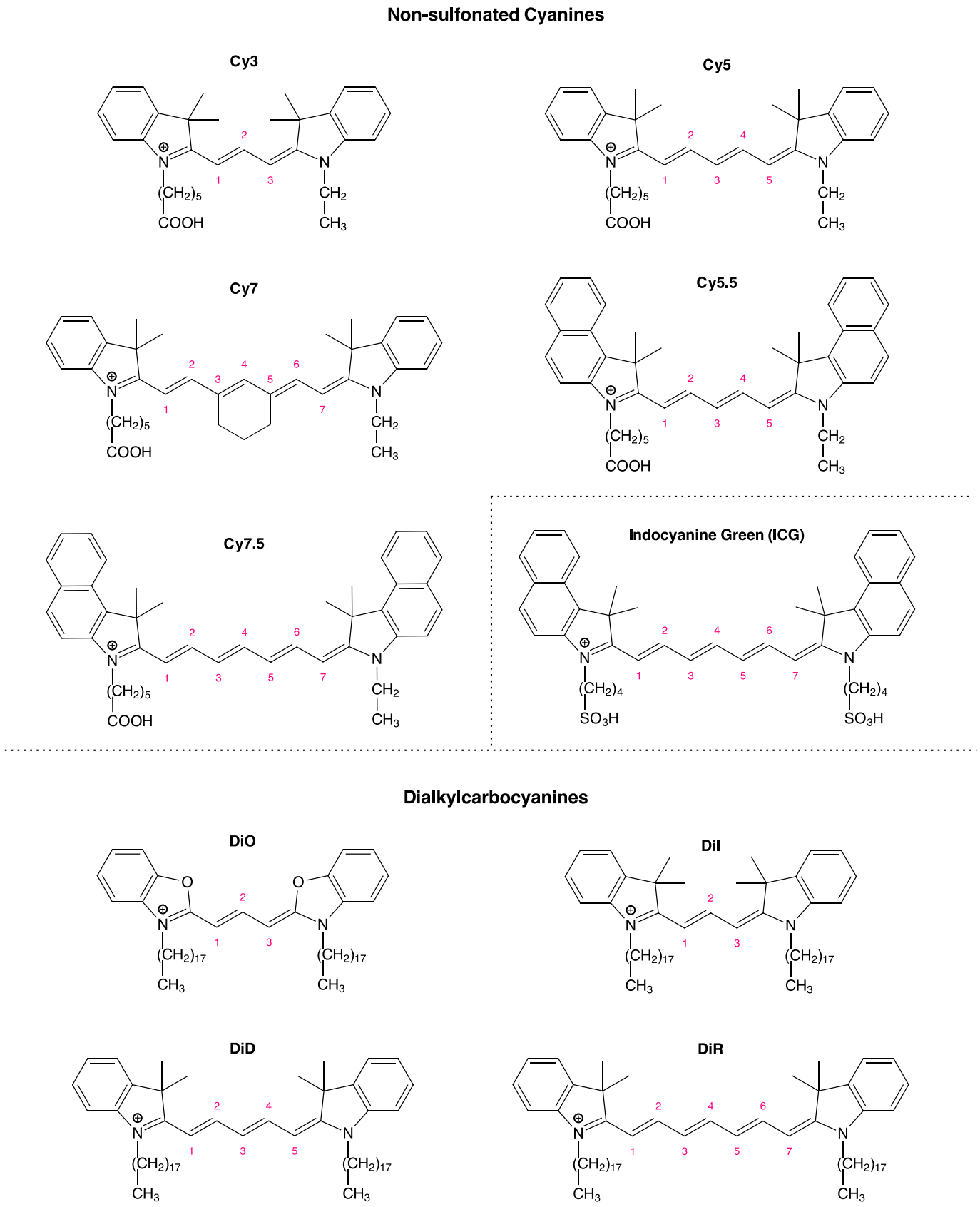


Fig. 3. Example of commonly used carbocyanine dyes for FRET with the emission spectrum in the range from 500 to 900 nm. Non-sulfonated cyanine dyes include Cy3 [35], Cy5 [36], Cy7 [37], Cy5.5 [38], Cy7.5 [38], and ICG [39]. Dialkylcarbocyanine dyes include DiO, DiI, DiD, DiR [34]. There are structural similarities between Cy3/DiI, Cy5/DiD, Cy7/DiR, and Cy7.5/ICG. A longer polymethine chain (marked by carbon number) red-shifts the excitation and emission wavelengths towards the near-infrared region. (For interpretation of the references to colour in this figure legend, the reader is referred to the web version of this article.)

Table 1
Summary of the instrumental technique of FRET for *in vivo* pharmacokinetic study.

Instruments	Fluorometer/ microplate reader	Confocal Microscopy (CFM)	*In vivo* imaging system (IVIS)
Samples	• Plasma extract • Blood	• Tissue slice • Cells • Mouse's earlobe and liver vasculatures (*in vivo* intravital) • Zebrafish larva (whole-body)	• Mouse or rat (whole-body, live) • *Ex vivo* organs • Blood • Plasma extract
Assay technique	Semi-quantitative particle concentration and chemical assay	Qualitative & Semi-quantitative imaging assay	• Qualitative & Semi-quantitative imaging assay (live) • Semi-quantitative particle assay
Pharmacokinetic study	• Plasma particle concentration (SQT) • Particle stability in plasma (SQT)	• Particle stability in organ (QL, SQT) • Biodistribution (SQT) • Oral absorption (QL) • Cargo release (QL)	• Particle stability in organ or whole-body (QL, SQT) • Biodistribution (QL, SQT) • Plasma particle concentration (SQT) • Oral absorption (SQT) • Cargo release (SQT)
Advantages	• Gives a high-resolution fluorescence spectrum • True chemical assay • Potential for true quantitative analysis if done with proper calibration curves	• High image resolution (microscopic level) • More practical for qualitative imaging analysis	• Live animal whole-body image • Wide range of samples
Limitations	• Limited to plasma or blood sample • Non-imaging analysis	• Practical only for microscopic sample • Less practical for live animal imaging	• Signal interferences for whole-body imaging • Requires complex signal calibration procedures for FRET

QL = Qualitative assay.
SQT = Semi-quantitative assay.

its fluorochrome property and thus needs another FRET system from the pair of perylene and H_2TPyP.

3.5. Dendrimers

Dendrimers consisting of an inner core and a peripheral shell are the well-designed branching architectures macromolecules with abundant terminal groups allowing for dye conjugation. Dyes can also be loaded into the inner core.

PEG^{5k}-CA_8 telodendrimers were a class of dendrimer developed by Li et al. [54]. The basic structure of the telodendrimers consists of the PEG^{5k} moiety and the dendritic oligomer of cholic acid (CA_8). It is a self-assembly system in which cholic acid telodendrimers coalesce together as a hydrophobic core and the PEG^{5k} moiety facing outward as a hydrophilic shell. Carbocyanine dye DiO as the FRET donor was encapsulated in the core, while rhodamine B as the FRET acceptor was conjugated to the telodendrimer (Fig. 8).

4. *In vivo* pharmacokinetic studies using FRET-nanomedicine

Pharmacokinetic study involves collecting the animal's blood sample, tissues, organs, or even full-body imagery. In these different samples, FRET measurement can be performed by common fluorescence imaging tools, namely microplate reader, fluorometer, confocal microscopy (CFM), or *in vivo* imaging system (IVIS). All the instruments can perform the semi-quantitative assay, while only CFM and IVIS can perform qualitative and semi-quantitative imaging analysis. The advantages and limitations of each instrumental technique are summarized in Table 1. The following sections will detail these FRET techniques used as the *in vivo* nanoparticle tracker exemplified with some nanoparticles described before. Table 2. summarizes all the FRET system and their application for the *in vivo* pharmacokinetics of the nanomedicine.

4.1. FRET in vivo nanoparticle tracking by confocal microscopy (CFM)

CFM is used for the tissue slides or organ samples. CFM may also be used for live imaging of the superficial veins of rodents, or the whole body of zebrafish larvae.

4.1.1. Live-imaging of the vasculature by intravital FRET-CFM

Live-imaging of the vasculature by intravital FRET-CFM was only performed on micelles nanoparticles.

Chen et al. [40] were the first to utilize FRET as the *in vivo* nanoparticle tracker. The technique was to perform the qualitative imagery assay and the semi-quantitative assay on the *in vivo* particle stability of the PED-b-PPLG micelles (PPMs) in a mouse model. Then the FRET-PPMs were intravenously injected into the mice. The fluorescence image of the vasculature on the mouse's ear lobe was taken by the confocal microscope. The intensity of the signals from the photo was recorded, and the FRET proximity ratio could be calculated to estimate the plasma particle concentration of the micelles. The proximity ratio (called the FRET ratio) was also compared with the positive standard of the fully intact micelles in water and the negative standard of the dissociated micelles in acetone. The result showed the fast *in vivo* dissociation of FRET-PPMs in the mouse's circulatory system, as the PR dropped from 0.90 to 0.46 (negative control's PR = 0.30) within 15 min. Further *in vitro* particle stability study using the FRET method revealed that α- and β-globulins in blood were the probable cause of the PPMs' fast dissociation.

Later, by Ishizawa et al. [42], the *in vivo* live FRET imaging of FRET-PPMs in the mouse's ear and the liver vasculature was conducted by confocal microscopy for up to 4 h (Fig. 9.). The particle stability in the vasculature was observed qualitatively and found that FRET-PPMs extravasated to a hepatic tissue and dissociated. Further *in vitro* FRET experiment also revealed that FRET-PPMs might dissociate while interacting with the hepatic cell membrane.

A derivative of PEG-PDLLA was developed by Lee et al. [41] as the disulfide-bonded mPEG-(Cys)4-PDLLA micelles (DS-PPMs) for the delivery of doxorubicin, aiming for strengthening the particle integrity and for the targeting release in the glutathione (GSH) rich environment of the cancer tumor. Confocal microscopy was also utilized to record the vasculature on the mice's ear lobe. The *in vivo* particle stability of PPMs and DS-PPMs in the circulation system was semi-quantitatively analyzed by the proximity ratio (PR). The result was clear that the PR of DS-PPMs was always higher than the PPMs up to 12 h, meaning that DS-PPMs retained higher particle stability than PPMs. Next, the biodistribution and the particle stability of DS-PPMs (alone) in the tumor were studied using the same FRET confocal microscopy technique. M109 tumor grafted mice were intravenously injected with DS-PPMs with the tumor and internal organs harvested after 6 h. The particle integrity of the DS-

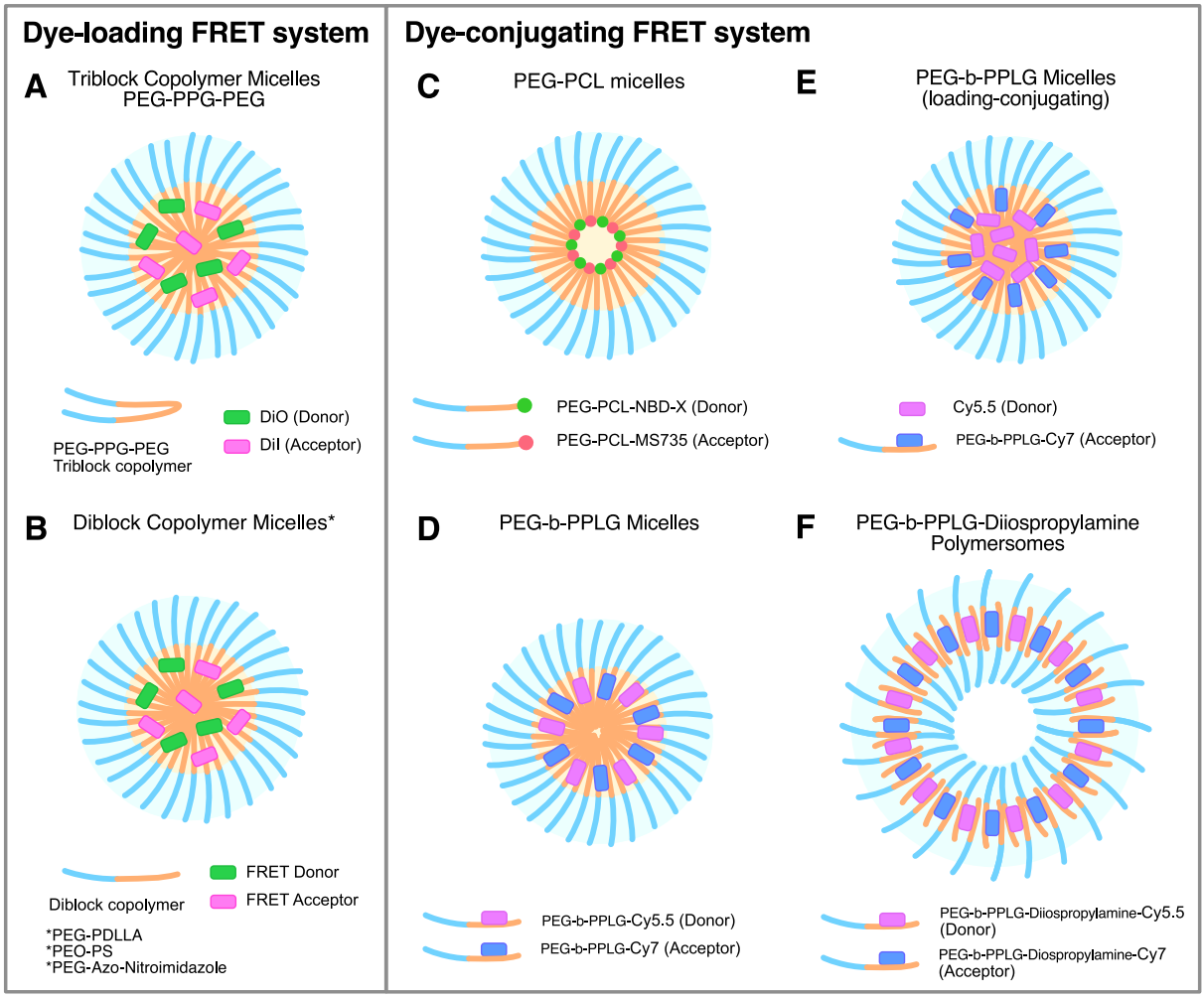


Fig. 4. Schematic illustration summarizing the FRET system of polymeric micelles. Nanoparticles with dye-loading FRET system include A) Triblock copolymer micelles PEG-PPG-PEG, B) Diblock copolymer micelles including PEG-PDLLA, PEO-PS, PEG-Azo-Nitroimidazole. Nanoparticles with dye-conjugating FRET system include C) PEG-PCL micelles, D) PEG-b-PPLG micelles with Cy5.5 and Cy7 conjugation, E) PEG-b-PPLG micelles with Cy5.5 loading and Cy7 conjugation, F) PEG-b-PPLG polymersomes with Cy5.5 and Cy7 conjugation.

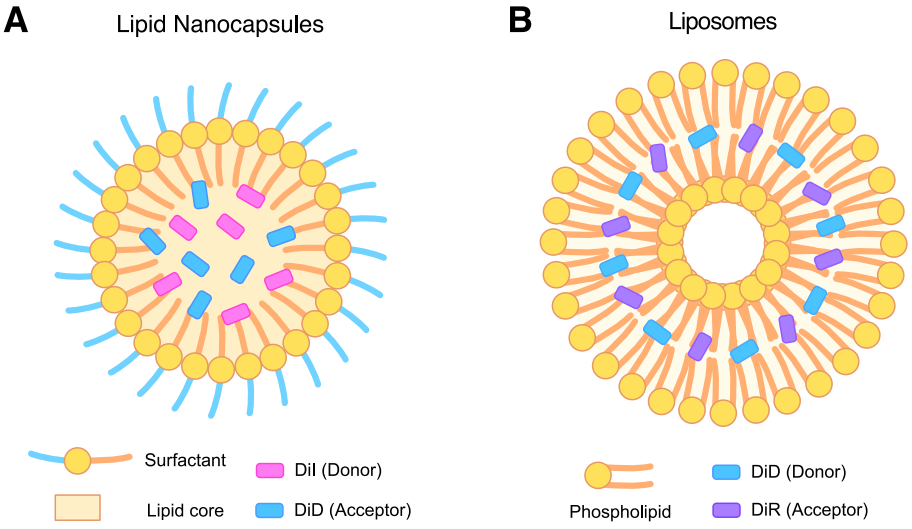


Fig. 5. Schematic illustration summarizing the published FRET system of lipid nanocapsules and liposomes. A) Lipid nanocapsules with the FRET system of DiI and DiD from Gravier et al. [29] as an example. B) Liposomes with the FRET system of DiD and DiR from Liu et al. [48] as an example. FRET dyes are co-encapsulated inside the lipid compartment of the nanoparticles.

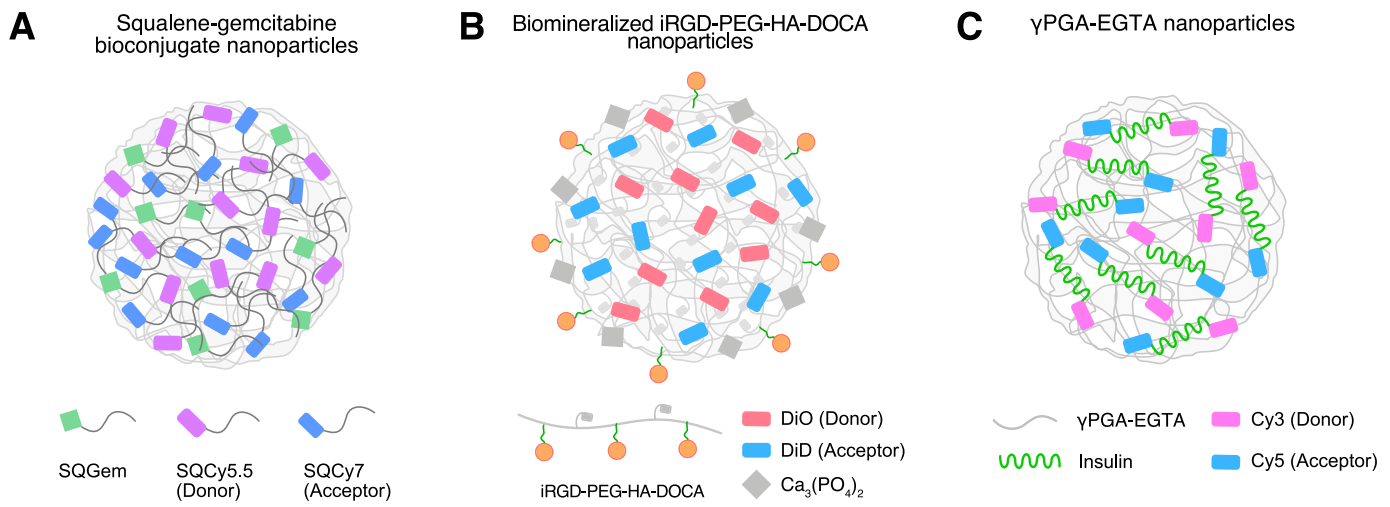


Fig. 6. Schematic illustration summarizing the published FRET system of the nanospheres. A) Squalene-gemcitabine bioconjugate nanoparticles with the FRET dye Cy5.5 and Cy7 conjugating to squalene. B) Biomineralized iRGD-PEG-HA-DOCA nanoparticles with the FRET dyes DiO and DiD loading inside the polymer matrix. C) γPGA-EGTA nanoparticles with the FRET dyes Cy3 and Cy5 conjugating to insulin ant then loaded inside the polymer matrix.

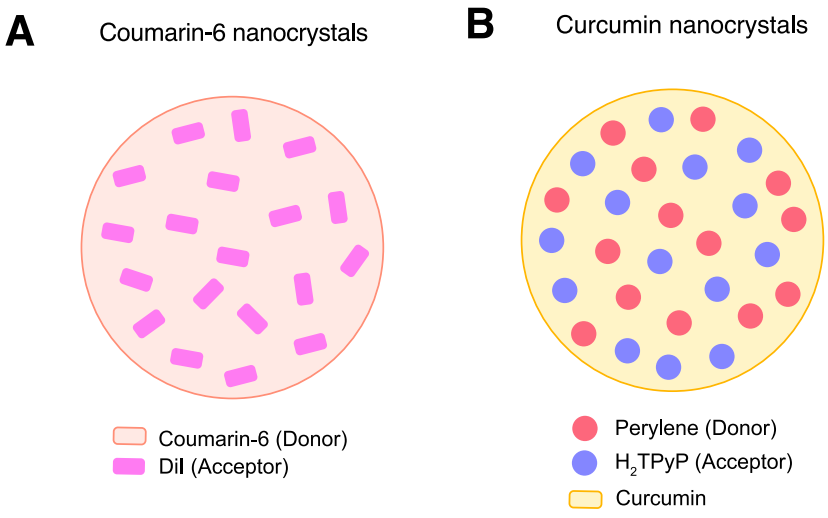


Fig. 7. Schematic illustration summarizing the published FRET system of the nanocrystals, in which FRET dyes are dispersed inside the nanocrystal. A) Coumarin-6 nanocrystals, which coumarin-6 itself acts as FRET donor to the acceptor DiI. B) Coumarin nanocrystal with the FRET system of perylene and H_2TPyP (porphyrin derivative).

PPMs was analyzed semi-quantitatively by FRET in the tumor vasculature *vs.* the tumor cells. DS-PPMs retained their integrity in the tumor vasculature (PR = 0.66) while dissociated in the tumor cell (PR = 0.31). FRET images from other *ex vivo* organs (liver, spleen, lungs, kidney) were analyzed qualitatively, and a strong FRET acceptor signal was visually observed. This means that DS-PPMs have a highly targeting release in the tumor. Further study on the efficacy of doxorubicin encapsulated DS-PPMs (DOX-DS-PPMs) showed a 7-times increase of doxorubicin accumulation in the tumor and higher tumor suppression efficacy, compared with the conventional non-disulfide doxorubicin encapsulated PPMs (DOX-PPMs), which had poorer *in vivo* particle stability. This study really demonstrated that the *in vivo* particle integrity of the nanocarrier really has an effect on drug efficacy and delivery, and FRET is proved as a very practical tool to investigate it.

These studies really demonstrated a series of technical development of FRET application for the live *in vivo* test using confocal microscopy. However, the intravital imaging of liver vasculature is rather complicating and invasive to the animal (an advanced surgical procedure to open a living rat's liver and keep them alive for an extended period of time).

4.1.2. *Imaging of ex vivo tissue slides by FRET-CFM*

For this technique, only liposome systems were described. Firstly, Tang et al. [55] performed the FRET semi-quantitative assay to investigate the particle stability of liposomes (LPs) *vs.* D-self-peptide-labeled liposomes (DSL) in the mouse's liver. DSL was designed to have a high adsorption affinity to the cell membrane of the various hepatic cells, blocking the hepatic cell's endocytosis and the hepatic clearance of the actual therapeutic nanoparticles that would be administrated later. As such, DSL was expected to have long particle stability on the liver cell membrane surface. For the FRET assay, carbocyanine dyes DiO (donor) and DiI (acceptor) were co-encapsulated inside the liposomes (LPs) voids. Mice were intravenously injected with the FRET-LPs and FRET-DSL. They were then sacrificed after 0.5, 4, 24 h with their liver harvested and sliced by a microtome. The FRET fluorescence image of the sliced liver sample was taken using a microplate reader. The fluorescence intensity was retrieved from the image allowing for the FRET proximity ratio to be calculated and normalized to the time zero (called

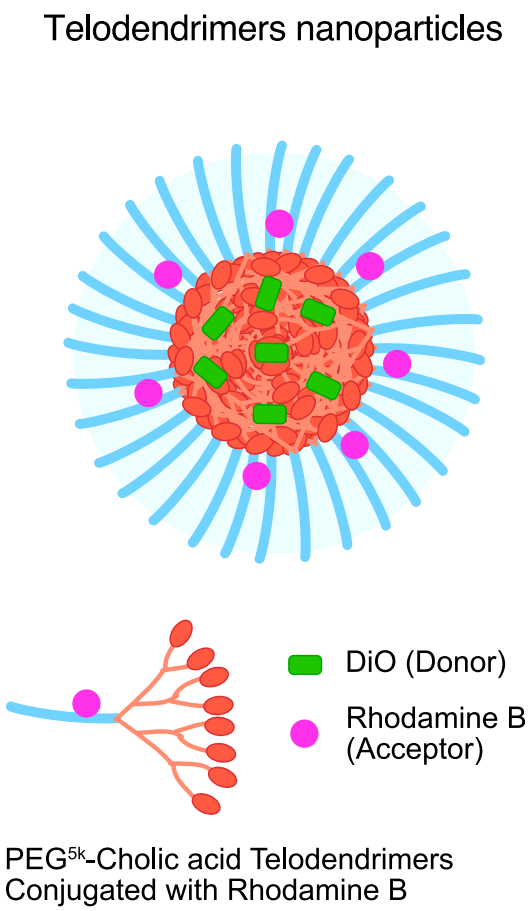


Fig. 8. Schematic illustration summarizing the FRET system of telodendrimers nanoparticles. DiO was loaded to the cholic acid core, and rhodamine B was covalently conjugated to telodendrimers. Adapted with permission from [54], Copyright 2012 American Chemical Society.

% relative FRET ratio). FRET-DSL was found to be more stable than FRET-LPs in the mouse's liver after 24 h, suggesting a slower elimination of DSL from the liver. DLS was later verified to be more effective than the conventional LPs to block the hepatic clearance of the amphotericin B encapsulated PLGA-Nanoparticles. This resulted in a prolonged circulation of amphotericin B and the increase in its effectiveness against the brain's fungal infection in a mouse model. This research again shows the usefulness of FRET to analyze the *in vivo* particle stability of LPs.

Liu et al. [48] also used the qualitative FRET imaging by confocal microscopy to study the oral absorption of liposomes (LPs). The jejunum section was selected for the *in vivo* intestinal epithelial uptake experiment. Male Sprague-Dawley rats were anesthetized, and the FRET-LPs were directly injected into the jejunum and ileum where the Peyer's patches were situated. After 2 h, the said intestinal section was harvested, immobilized, frozen, and further stained with DAPI for revealing tissue structure. Then, the intestinal sample was sliced and put under the CFM for magnified imaging. Its visible presence signified the intact FRET-LPs that migrated through the epithelium layer of jejunum and ileum. However, the FRET signal could not be quantifiable with the confocal microscopy, making this only the qualitative assay. It was observed that the intact cationic LPs and PEGylated LPs had a higher FRET intensity throughout the jejunum's epithelium, suggesting their better uptake.

4.1.3. FRET-CFM with zebrafish larva

4.1.3.1. Nanocrystals. Li et al. [52] demonstrated the use of qualitative FRET with the zebrafish larva model for the first time for investigating the particle stability of FRET-nanocrystal. The *in vivo* particle stability was qualitatively studied by exposing zebrafishes (*Danio rerio*) and their larvae with the FRET-nanocrystals using the incubation method. After a specific time period, fluorescence images of the fishes and the larvae were taken using confocal microscopy. The presence of the FRET acceptor signals in the imagery determines the presence of stable nanocrystals in the zebrafish larvae. Imaging results found the increase in FRET intensity signal over time 60 min indicating that the nanocrystal absorbed into the larva gradually. Unfortunately, FRET was only used qualitatively and briefly in this research, and only coumarin-6 (FRET donor) was further analyzed for their accumulation in organs regardless of the particle integrity.

4.1.3.2. Micelles. Another study using FRET with a zebrafish larva model was performed by Tao et al. [43]. The semi-quantitative FRET technique was employed to study the *in vivo* particle stability and the cargo release of the ordinary PEG-PPG-PEG micelles (OPMs) and the disulfide bond cross-link PMs (CPMs). The FRET-micelles were injected into the circulatory system of the zebrafish's larva using a microneedle. Over specific time points, the live fluorescence images of the fishes were taken by confocal microscopy. At first, the image was qualitatively analyzed by determining the presence of the FRET acceptor signal in the caudal veins and caudal arteries. Then, both the FRET donor and the FRET acceptor signals were quantified by the software (Fig. 10.). In this case, the FRET donor (DiO) signal means the released core content, and the FRET acceptor (DiI) signal determines the relative amount of the intact micelles. Then, the FRET proximity ratio was calculated and normalized to 100% (called % integrity), being used as another integrity parameter. CPMs were found to be more stable than PMs. After 1 h, CPMs retained 60% integrity in contrast to 30% integrity of OPMs. Next, in order to investigate the cargo release dynamic, the fluorescence intensity of the donor channel and FRET channel were directly compared in their arbitrary unit. In this article, the donor signal from DiO was considered the signal of the free DiO released from the OPMs, meaning that it was the measurement of the dequenching of DiO. Despite the fact that the donor dequenching may imply the release of the free donor dye, the donor (de)quenching intensity alone is not adequate as the proof of FRET [22], *i.e.*, not the proof of integrity or content release. As such, the donor intensity can be, at best, a qualitative parameter for the cargo release. Generally, the FRET proximity ratio is adequate for the determination of the cargo release dynamics.

4.2. FRET in vivo nanoparticle tracking by in vivo imaging system (IVIS)

For animals such as rats or mice, the IVIS allows for live imaging of either whole-body animals, *ex vivo* organs, or even blood samples. It also comes with the quantification software to quantify the emission intensity from the area of interest in the image allowing both qualitative imagery and semi-quantitative assay.

4.2.1. FRET-IVIS for live whole-body and ex vivo organs imaging

4.2.1.1. Micelles. Zou et al. [44] demonstrated the use of a semi-quantitative FRET assay for the first time using IVIS to study the cargo release of PEO-PS micelles. For this experiment, FRET was measured from two perspectives. The first perspective is like an ordinary FRET system in which DiD and DiR were co-loaded into the micelles and administrated to the test subject. Then, decreasing FRET signals signifies the cargo release or the micelle dissociation. Nevertheless, to focus on the released content, this conventional co-loaded system has a drawback. Because, if the released dyes still accumulate together, they will still give too bright a FRET signal that makes it very difficult to be distinguished from the FRET of the intact micelle. Therefore, the second perspective was developed to fix this problem. This time, DiD and DiR

Table 2
Summary of the FRET system used for pharmacokinetic studies of nanomedicine.

Nanoparticle type	FRET system				Instrument	Animal model	Area of Interest	Pharmacokinetics study	Level of assay	Reference
	Donor/ Acceptor pair	FRET Excitation (nm)	Donor Emission (nm)	Acceptor Emission (nm)						
Nanospheres										
SQGem	Cy5.5/Cy7.5	640	695–770	810–875	IVIS	Mouse	Liver	Particle stability in liver	Semi-quantitative	[38]
iRGD-PEG-HA-DOCA	DiO/DiD	484	501	565	Fluorimeter	Rat	Plasma extract	Plasma particle concentration, particle stability	Semi-quantitative	[49]
γPGA-EGTA	Cy3/Cy5	535	570	680	IVIS	Rat	Duodenum	Protective effect of the nanoparticle against the intestinal enzyme	Qualitative, Semi-quantitative	[50,51]
Nanocapsules										
LNCs, LNEs	DiD/FC730-C18	590	660	764	IVIS	Mouse	Whole-body (live), *ex vivo* organs	*In vivo* particle stability, Biodistribution	Qualitative	[56]
LNCs	DiI/DiD	535	640	680	IVIS	Mouse	Liver, Tumor	*In vivo* particle stability, Biodistribution	Semi-quantitative	[29]
					CFM	Mouse	Tumor	*In vivo* particle stability, Biodistribution	Semi-quantitative	[29]
LNEs	Cy5.5TPB/ Cy7.5TPB	640	700	820	IVIS	Mouse	Whole-body (live), Tumor	*In vivo* particle stability, Biodistribution	Semi-quantitative	[57]
Liposomes										
Liposomes	DiD/DiR	640	n/a	780	IVIS	Mouse	Intestines, hearts, liver, spleen, kidney, lungs (*ex vivo*)	Particle stability in the GI, oral absorption, biodistribution	Semi-quantitative	[48]
					CFM	Rat	Intestines	Oral absorption	Qualitative	[48]
Liposomes	DiO/DiI	435–460	470–515	515–580	CFM	Mouse	Liver	Particle stability in liver	Semi-quantitative	[55]
Nanocrystals										
Coumarin-6 nanocrystals	Coumarin-6/ DiI	488	490–540	555–675	CFM	Zebrafish larva	Whole-body (intravital)	*In vivo* particle stability	Qualitative	[52]
Curcumin nanocrystals	Perylene/ H_2TPyP	n/a	n/a	635	Microplate reader	Mouse	Plasma extract	Plasma particle concentration	Semi-quantitative	[53]
					IVIS	Mouse	*Ex vivo* organs and tumor	Biodistribution	Semi-quantitative	[53]
Polymeric micelles (dye-loading FRET system)										
PEG-PPG-PEG	DiO/DiI	488	508	578	CFM	Zebrafish larva	Cauda (intravital)	*In vivo* particle stability	Semi-quantitative	[43]
								Cargo release	Qualitative	[43]
PEG-PDLLA	DiO/DiI	488	501	565	CFM	Mouse	Ear vasculature (intravital)	Particle stability in blood circulation	Qualitative, Semi-quantitative	[40]
PEG-PDLLA	DiD/DiR	640	680	809	CFM	Mouse	Ear and liver vasculature (*in vivo* intravital)	*In vivo* particle stability	Qualitative	[42]
					IVIS	Mouse	Whole-body (live), *ex vivo* organs	*In vivo* particle stability, Biodistribution	Qualitative, Semi-quantitative	[42]
mPEG-(Cys)4-PDLLA	DiO/DiI	488	500–530	555–655	CFM	Mouse	Ear vascular	*In vivo* particle stability in blood circulation	Qualitative, Semi-quantitative	[41]
							Ex vivo tumor & organs	Biodistribution, Particle stability	Qualitative, Semi-quantitative	[41]
PEO-PS	DiD/DiR	640	680	780	IVIS	Mouse	Whole-body (live)	Cargo release (reversed FRET), Particle stability	Semi-quantitative	[44]
	Cy5/Cy7	640	670–730	730–790	IVIS	Mouse	Tumor	Cargo release	Semi-quantitative	[30]

(*continued on next page*)

Table 2 (*continued*)

Nanoparticle type	FRET system				Instrument	Animal model	Area of Interest	Pharmacokinetics study	Level of assay	Reference
	Donor/ Acceptor pair	FRET Excitation (nm)	Donor Emission (nm)	Acceptor Emission (nm)						
PEG-Azo-Nitroimidazole										
Polymeric micelles (dye-conjugating FRET system)										
PEG-PCL	NBD-X/MS735	475	535	735	Fluorimeter	Mouse	Plasma extract	Plasma particle concentration	Semi-quantitative	[47]
PEG-b-PPLG	Cy5.5/Cy7	640	700	800	IVIS	Mouse	Whole-body (live), blood, *ex vivo* organs	Plasma particle concentration, Biodistribution	Semi-quantitative	[45,46]
Dendrimers										
TEMPO-PEG5k-CA8 telodendrimer	DiO/ Rhodamine B	480	530	580	Microplate reader	Mouse	Blood	*In vivo* particle stability, Plasma particle concentration	Semi-quantitative	[54]

CFM = confocal fluorescence microscopy.
IVIS = *In vivo* imaging system.
DiO = $DiOC_{18}(3)$ 3,3'-Dioctadecyloxacarbocyanine perchlorate.
DiI = $DiIC_{18}(3)$ 1,1'-Dioctadecyl-3,3,3',3'-Tetramethylindocarbocyanine perchlorate.
DiD = $DiIC_{18}(5)$ 1,1'-Dioctadecyl-3,3,3',3'-Tetramethylindodicarbocyanine perchlorate.
DiR = $DiIC_{18}(7)$ 1,1'-Dioctadecyl-3,3,3',3'-Tetramethylindotricarbocyanine iodide.
FC730-C18 = Interchim FluoProbes® 730 conjugated with octadecylamine.
TPB = tetraphenyl borate.
H_2TPyP = 5,10,15,20-tetro(4-pyridyl)porphyrin.
NBD-X = NBD-X, SE, Succinimidyl 6-(N-(7-Nitrobenz-2-Oxa-1,3-Diazol-4-yl)Amino)Hexanoate.
MS735 = Azide MegaStokes dye 735, 1-(3-Azidopropyl)-4-{2-[6-(diethylamino)-2-benzofuranyl]ethenyl}-3-sulfo-pyridinium inner salt.

were separately loaded into the micelles, making the DiD-micelles and the DiR-micelles. Then they were mixed with the same proportion and administered to the test subject. Thus, this is like a reversed FRET measurement that there is no FRET at the beginning. And then, the increase in FRET signals would only signify the released content, making it more sensitive than the co-loaded FRET system in studying the release dynamics. These techniques could be used for either *in vitro* or *in vivo* release studies. For the *in vivo* study, mice were divided into two groups, with one injected with the FRET-PEO-PS (the ordinary FRET system) and the other with the DiD-PEO-PS and DiR-PEO-PS mixture (the reversed FRET system). IVIS was used to obtain the full-body image and the fluorescence intensity value for calculating the FRET proximity ratio (PR, called FRET ratio in the article). The PR from the ordinary FRET system would decrease while the PR from the reversed FRET would increase. Thus, over time, the PR from the two FRET perspectives would meet and become equal, from which it indicates the end of the cargo release (Fig. 11). The difference between the ordinary PR and the reversed FRET PR could be calculated giving the release kinetics value, where the release half-life of FRET-PEO-PS was found to be 9.2 min in a mouse model. However, this release kinetic was too fast and inefficient for drug delivery to the tumor site. Thus, the oleic acid-coated iron oxide nanoparticles (IONPs) were incorporated into FRET-PEO-PS (becoming FRET-PEO-PS-IONP) to increase the lipophilicity of the nanocarriers. This strategy was proved to be successful as the release kinetics half-life measured by the same FRET-IVIS technique was found to be 50.8 min. Increasing lipophilicity of PEO-PS could slow down the premature release and hence improves drug delivery to the tumor. Thus, this study successfully demonstrated an advanced application of the semi-quantitative FRET technique to determine the cargo release kinetics with the benefit of live imagery using IVIS. It would be very interesting to develop further the quantitative technique based on this approach because this technique really allows both particle stability and release kinetics of the nanoparticles to be determined.

Morton and Quadir et al. [46] demonstrated the use of FRET semi-quantitative assay on the particle stability, biodistribution, and cargo release of PEG-b-PPLG micelles (PPMs). Basically, the dye-conjugating FRET system was used as a standard as Cy5.5 and Cy7 were both conjugated to PPLG and then mixed together to form the co-conjugated FRET-micelles (FRET-CPPMs), which represents blank-micelles. Moreover, the mixed system was employed, as Cy5.5 (donor) was loaded into the Cy7-conjugating micelles (FRET-PPM-Cy7) representing drug loading-micelles. Technically, the co-conjugated dye system determined only the dissociation of the micelles, while the mixed system allowed the determination of both dissociation and cargo release. However, in the pharmacokinetics study, they practically gave the same information of micelles stability since micelles dissociation and cargo release occur at the same time. For this experiment, the FRET assay was performed on a mouse model using both FRET dye systems in comparison to each other. Mice were intravenously injected with FRET-CPPM and FRET-PPM-Cy7. The relative plasma particle concentration of FRET-CPPMs and FRET-PPM-Cy7 was determined by two methods, both using IVIS. The first was by the FRET intensity obtained from the live full-body image (Fig. 12A). The FRET proximity ratio (PR) was calculated and normalized to the percentage called % FRET efficiency (Fig. 12C). The second was by the FRET intensity from the blood sample (Fig. 12B). PR was then normalized to the percentage of the initial PPMs concentration called % injected dose (%ID) (Fig. 12D). The result suggested that both the % FRET efficiency and the %ID were correlated and in accordance. The information from the %ID was more accurate because it came directly from blood with less signal interference from skin or other organs. As such, the blood clearance half-life of the micelles was obtained (Fig. 12D). In addition, the biodistribution was also studied using IVIS. Internal organs, including the mice's blood, were harvested for FRET intensity measurement. The result indicated a high accumulation of the intact micelles in the liver. This study really showed the flexibility and utility of IVIS with different experimental techniques to semi-

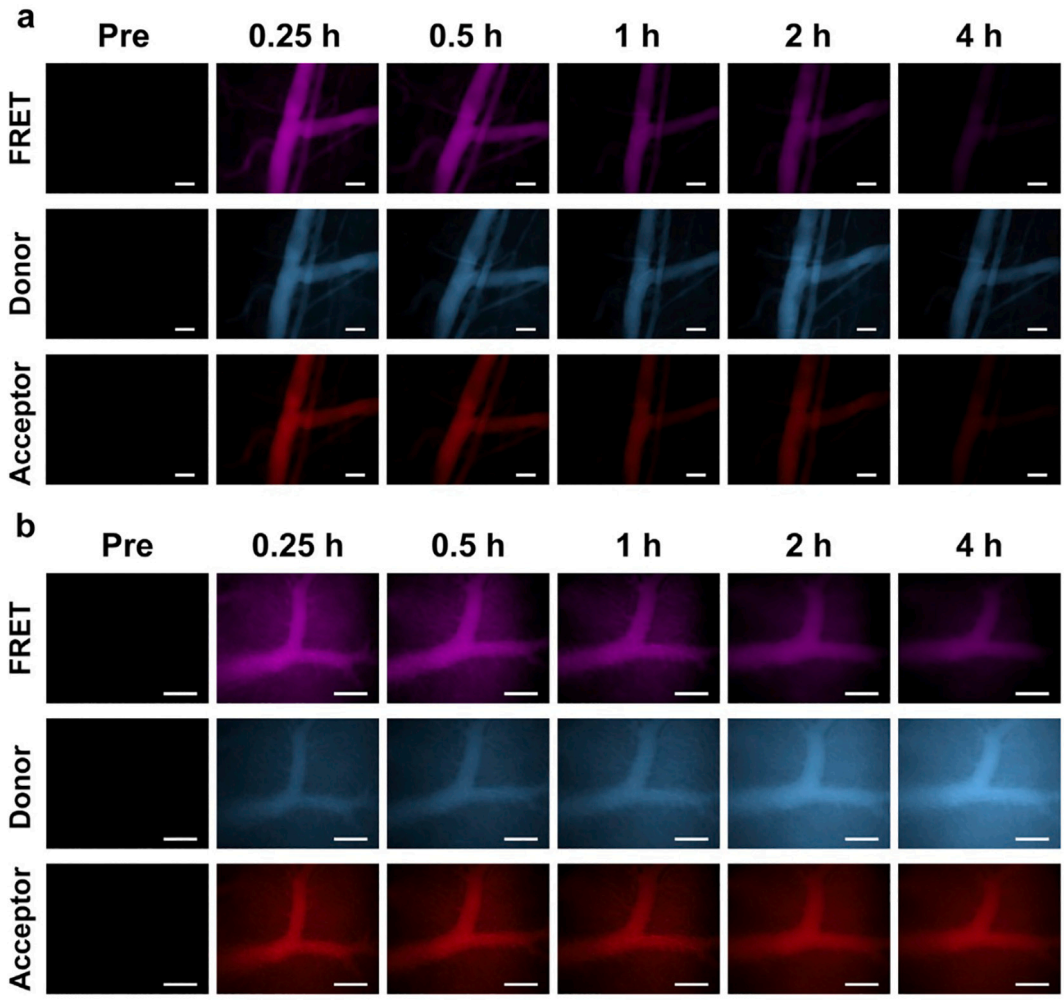


Fig. 9. An example of qualitative live *in vivo* FRET imaging analysis using confocal microscopy, by Ishizawa et al. [42]. PEG-PDLLA micelles were analyzed for the *in vivo* particle stability and biodistribution to the liver. A) FRET images of mouse's earlobe vasculatures. B) FRET images of mouse's liver vasculatures. The Figure shows that the FRET signal of FRET-PEG-PDLLA was found outside liver vasculature suggesting the intact nanoparticle's extravasation to liver cells. A drop in FRET signal and increase in donor signal in liver cells at 4 h also indicates nanoparticle's dissociation in liver cells. Reprinted from [42], Copyright 2020, with permission from Elsevier and American Pharmacist Association.

quantitatively analyze the plasma particle concentration and biodistribution by FRET.

Then, Ishizawa et al. [42] improved the semi-quantitative FRET technique used for PEG-PDLLA by using IVIS to capture the live full-body image of a mouse. DiD/DiR FRET system has a FRET acceptor emission spectrum closer to the near-infrared range than DiO/DiI system providing a higher tissue penetration ability, which is more suitable for the live full-body imagery. Mice were injected with FRET-PPMs. The FRET fluorescence signals were taken from the mice's chest and abdomen area, as well as the *ex vivo* organs at several time points up to 8 h. With the quantification software, IVIS gave the average intensity value. Thus, the FRET proximity ratio (called FRET ratio in the article) of the whole-body and *ex vivo* organs image signals was calculated. Then, the particle stability and the biodistribution were semi-quantitatively determined. The proximity ratio was calibrated with FRET-PPMs in PBS as the positive control and the one in ethanol as the negative control of the integrity. FRET-PPMs were found to dissociate over time with high accumulation in the liver and the lungs.

Finally, PEG-Azo-Nitroimidazole is a hypoxia-responsive micelle developed by Guo et al. [30] for drug delivery to the hypoxic environment of a tumor. Tumor-bearing mice were used in this experiment, and the FRET-micelles were directly administrated into the tumor. After specific time points, the IVIS was employed to take the live fluorescence image of the tumor. The ratio between the intensity of the FRET acceptor and the donor was calculated and used as the semi-quantitative parameter for the cargo release. The intensity ratio of the nitroimidazole micelles was found to have a greater decrease when compared to the nitroimidazole-free micelles (control), suggesting a better cargo release of the nitroimidazole micelles in the tumor environment. The *in vivo* FRET technique helped to prove the hypoxia-responsive efficacy of the nitroimidazole micelles, which was one of the most important aims of this study.

4.2.1.2. Polymersomes. Quadir and Morton et al. [45], developed PEG5k-b-PPLG-Diiospropylamine (PPD) polymersomes developed. Unlike the normal PEG-b-PPLG, this polymer rearranges into a bilayer and becomes polymersomes with PEG to form an outer shell. The PPD-polymersomes are also designed to be acid pH-responsive dissociation, aiming for drug release in the acidic environment of a cancer tumor. The FRET intensity from *ex vivo* organs and blood samples was measured by IVIS and normalized with that of the injected dose to become the % injected dose (%ID). Thus, the semi-quantitative biodistribution data and the relative particle concentration of the intact FRET-PPD-polymersomes in a tumor-bearing mouse model were provided. The intact FRET-PPD-polymersomes were found to accumulate in the liver at 21%ID and in the tumor at 3%ID after 24 h. Doxorubicin-loaded PPD-

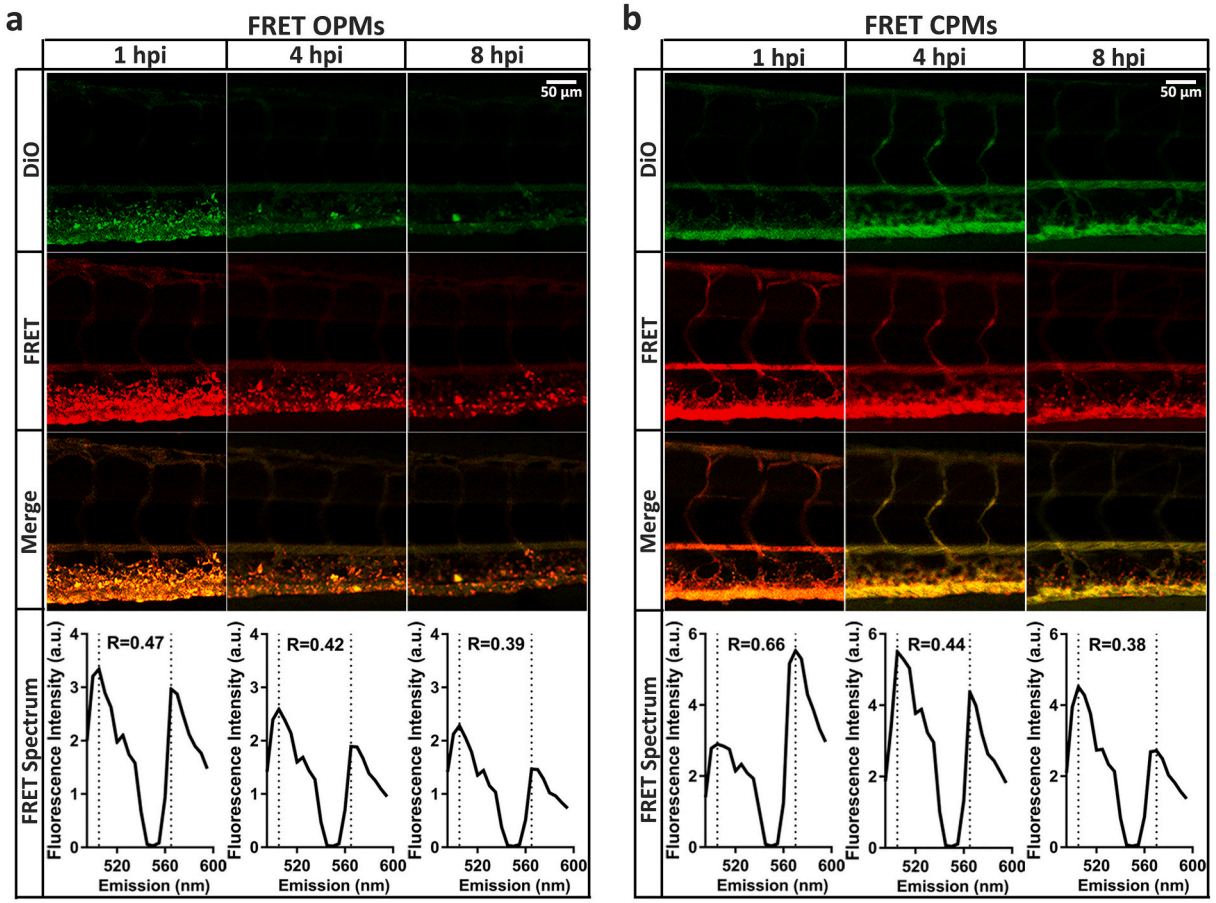


Fig. 10. An example of a semi-quantitative FRET live imaging assay in zebrafish larva model using confocal microscopy, by Tao et al. [43]. PEG-PPG-PEG micelles (PMs) were analyzed for the *in vivo* particle stability. A) Live FRET imaging of the ordinary PMs (OPMs) and B) Live FRET imaging of the disulfide bond cross-link PMs (CPMs). FRET signal of FRET-CPMs was stronger than FRET-OPMs after 1 h, suggesting higher stability of FRET-OPMs due to the disulfide bond cross-link. The bottom row shows the FRET spectra in terms of proximity ratio, which was semi-quantified as %integrity. Reprinted from [43], Copyright 2020, with permission from Elsevier.

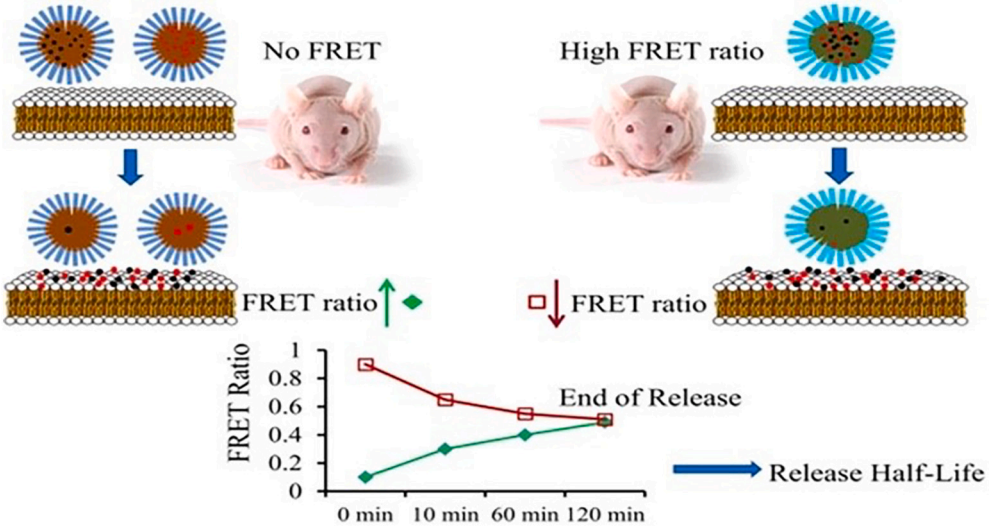


Fig. 11. Schematic illustration summarizes the released dynamic study using the reversed FRET technique developed by Zou et al. [44]. Reprinted with permission from [44], Copyright 2013 American Chemical Society.

polymersomes also showed a tumor suppression effect in mice when compared to the untreated group.

4.2.1.3. Lipid nanoparticles. Lainé et al. [56] developed the FRET technique to qualitatively study the biodistribution of lipid nanocapsules (LNCs), DSPE-mPEG-2000 lipid nanocapsules (DPEG-LNCs),

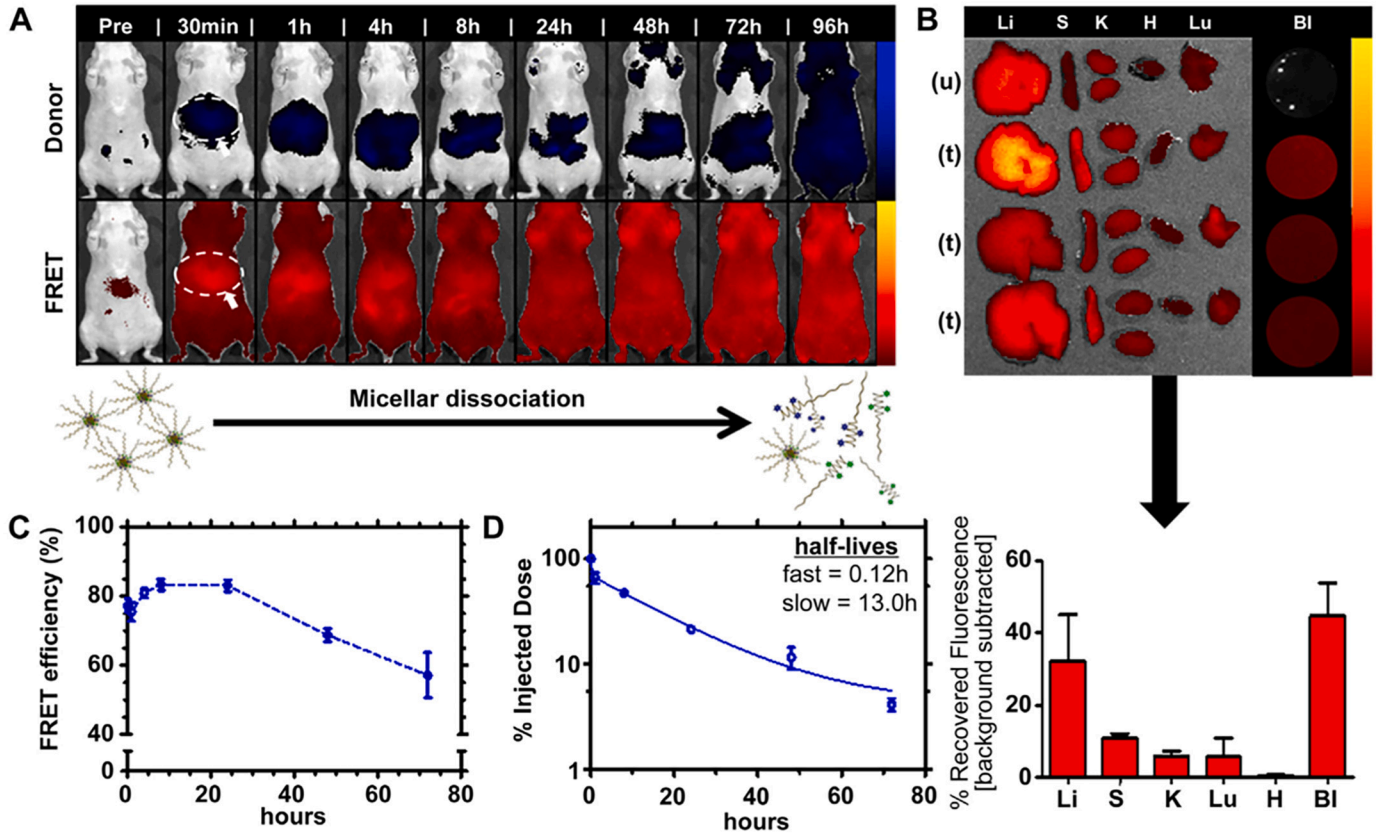


Fig. 12. An example of semi-quantitative FRET imaging analysis in a wide range of samples from mouse model using IVIS, by Morton et al. [46]. PED-b-PPLG micelles (PPMs) were analyzed for the *in vivo* plasma particle concentration and biodistribution. A) Live whole-body FRET IVIS image analysis showing the biodistribution of intact micelles. B) FRET IVIS image analysis of *ex vivo* organs: liver (Li), spleen (S), kidney (K), heart (H), lungs (Lu), and blood (Bl) showing the organ biodistribution and particle stability in the circulatory system. C) PR (called % FRET efficiency in the article) of the blood sample analyzed by IVIS. D) PR normalized to the percentage of the initial PPMs concentration called % injected dose (%ID) with the blood clearance half-life calculated following the two-compartment pharmacokinetics model. Reprinted from [46], Copyright 2014, with permission from Elsevier.

and lipid nanoemulsions (LNEs). The pair of FRET dyes were co-encapsulated inside the LNCs, DPEG-LNCs, and LNEs. These FRET nanoparticles were intravenously injected into nude mice. Using IVIS, the fluorescence image of the mice was recorded over time from the FRET channel and free FP730-C18 (acceptor dye) channel. The image deconvolution technique was employed to differentiate the three emission signals from each other by calibrating each signal with the signal from FRET-LNCs *vs.* the mixture of DiD-LNCs FP730-C18-LNCs (likewise for LNEs); and then converting them to pseudocolors. The visible presence of FRET pseudocolors over the area of the mice's body signified the accumulation of FRET nanoparticles in the internal organ beneath the area. As such, the biodistribution of FRET-LNCs, FRET-DPEG-LNCs, and FRET-LNEs to the organs could be identified qualitatively. Image results of the whole rat body showed that FRET-DPEG-LNCs and FRET-LNEs had a different biodistribution from the conventional FRET-LNCs. However, the whole-body image alone can only give an approximative and inconclusive result for the particle's biodistribution because the superficial signals from the skin can obscure the signal from deeper organs. As a result, IVIS images of the *ex vivo* organs and the blood were taken to detail the biodistribution. Then, it was revealed that the intact FRET-DPEG-LNCs had better particle stability in blood at 3 h and less accumulation in the liver after 24 h when compared with FRET-LNCs. In conclusion, this IVIS FRET technique could give a qualitative study of the biodistribution and particle stability of the LNCs and LNEs. However, even though the IVIS is a quick and non-invasive technique for the qualitative assay, the obtained result is inadequate. As such, *ex vivo* organ imaging is still needed for meaningful interpretation. Finally, a more complex semi-quantitative FRET technique using the IVIS was also used by Gravier et al. [29] for the particle stability and the biodistribution of LNCs in the liver and the breast carcinoma tumors. The FRET dyes were also co-encapsulated inside LNCs or LNEs. The FRET nanoparticles were intravenously injected into nude mice with TS/A-pc breast carcinoma tumors. Using the IVIS, FRET was recorded around the liver and the tumor area. The signals were corrected for the autofluorescence background prior to the injection. Then, the FRET ratio between the acceptor and the donor signals could be calculated from the image as *FRET Ratio = DiD (Acceptor) signal / DiI (donor) signal* and then converted to the percentage of intact FRET nanoparticles (called % intact LNCs) *via* the calibration curve. The calibration curve of the % intact FRET nanoparticles could be constructed by mixing FRET nanoparticles with various concentrations of DiI-LNCs and DiD-LNCs mixture ranging from 100% FRET to 0% FRET (100% of DiI-LNCs and DiD-LNCs mixture). This DiI-LNCs and DiD-LNCs mixture simulated the remnants of FRET-LNCs when the FRET dyes DiI and DiD were far apart and yielded no FRET. As such, the % intact LNCs in the liver and the tumor was obtained. Around 45% of intact LNCs were founded both in the liver and the tumor after 1 h and then dropped in half after 5 h. After 24 h, around 5% of the intact LNCs were detected in the tumor but 0% in the liver, indicating that LNCs were less stable in the liver than in the tumor. Furthermore, the % intact LNCs of the *ex vivo* tumor was determined using the same method but with confocal microscopy. A similar result was obtained, confirming the results from IVIS. Summarily, this research demonstrated the use of FRET by both the IVIS and the confocal microscopy to semi-quantitatively study the biodistribution and the particle stability in mice's liver and tumor.

4.2.1.4. Nanocrystals. FRET-curcumin nanocrystals were also developed by Zhang et al. [53] (called the co-doped curcumin nanoparticles in the article), aiming for their theragnostic application. Curcumin is a fluorophore, but in a nanocrystal form, it does not emit fluorescence. Therefore, FRET was instead employed as the nanocrystal tracker. As such, the FRET pair of perylene (donor) and 5,10,15,20-tetro(4-pyridyl) porphyrin (H_2TPyP, acceptor) was dissolved inside the curcumin nanocrystal. However, free curcumin dissolved from the nanocrystals can still give a fluorescence emission at 520 nm, and that can also be used as a direct parameter of free curcumin. By using IVIS, it allowed for the semi-quantitative assay of the biodistribution in a mouse model. The FRET-curcumin nanocrystal was intravenously injected into xenografted mice daily for 14 days. Then, the mice were sacrificed with their internal organs, including a xenografted tumor harvested. The FRET signal from H_2TPyP was then recorded by IVIS. However, the article does not clearly specify the excitation or the emission wavelength. Besides, the mean FRET intensity from each organ was obtained and compared with each other, revealing the relative amount of FRET-curcumin nanocrystal in each organ. The accumulation of the FRET-nanocrystal was found mainly in the liver and the tumor.

4.2.2. FRET-IVIS with pseudocolors technique

4.2.2.1. Lipid nanoparticles. Another similar IVIS technique was developed by Bouchaala et al. for lipid nanoemulsions (LNEs) [57]. This time, the FRET pair used was the carbocyanine Cy5.5 and Cy7.5 with a bulky counterion tetraphenylborate (TPB) added to increase their lipophilicity, making them Cy5.5TPB and Cy7.5TPB, which were employed as the donor and the acceptor respectively. By increasing the lipophilicity, the TPB-dye had a higher encapsulation capacity in the LNEs. In this study, FRET-LNEs were injected into the tumor-bearing mice. IVIS was employed for live whole-body imagery with the excitation at 640 nm, the FRET donor at 700 nm, and the FRET acceptor at 820 nm. FRET proximity ratio (PR) was calculated from the area of interest, which is the tumor and the liver areas, and then other *ex vivo* organs dissected from the mouse after 24 h. Several mixtures of donor-LNEs and acceptor-LNEs were used to calibrate the PR to the pseudocolors and then converted it to the % integrity that could overlay on the IVIS image (Fig. 13). So, unlike the previous technique, this technique not only showed the plain FRET intensity but showed the pseudocolors of the particle integrity itself on the image. The result indicated that the new TPB-dye gave a higher spatial resolution for IVIS, allowing for the semi-quantitative % integrity of the FRET-LNEs in the liver and the tumor area to be determined over time. The biodistribution from the *ex vivo* organs also showed a high accumulation of the intact FRET-LNEs and the in the liver and the tumor. This last study really demonstrated an impressive improvement in the FRET system for lipid-nanoparticles.

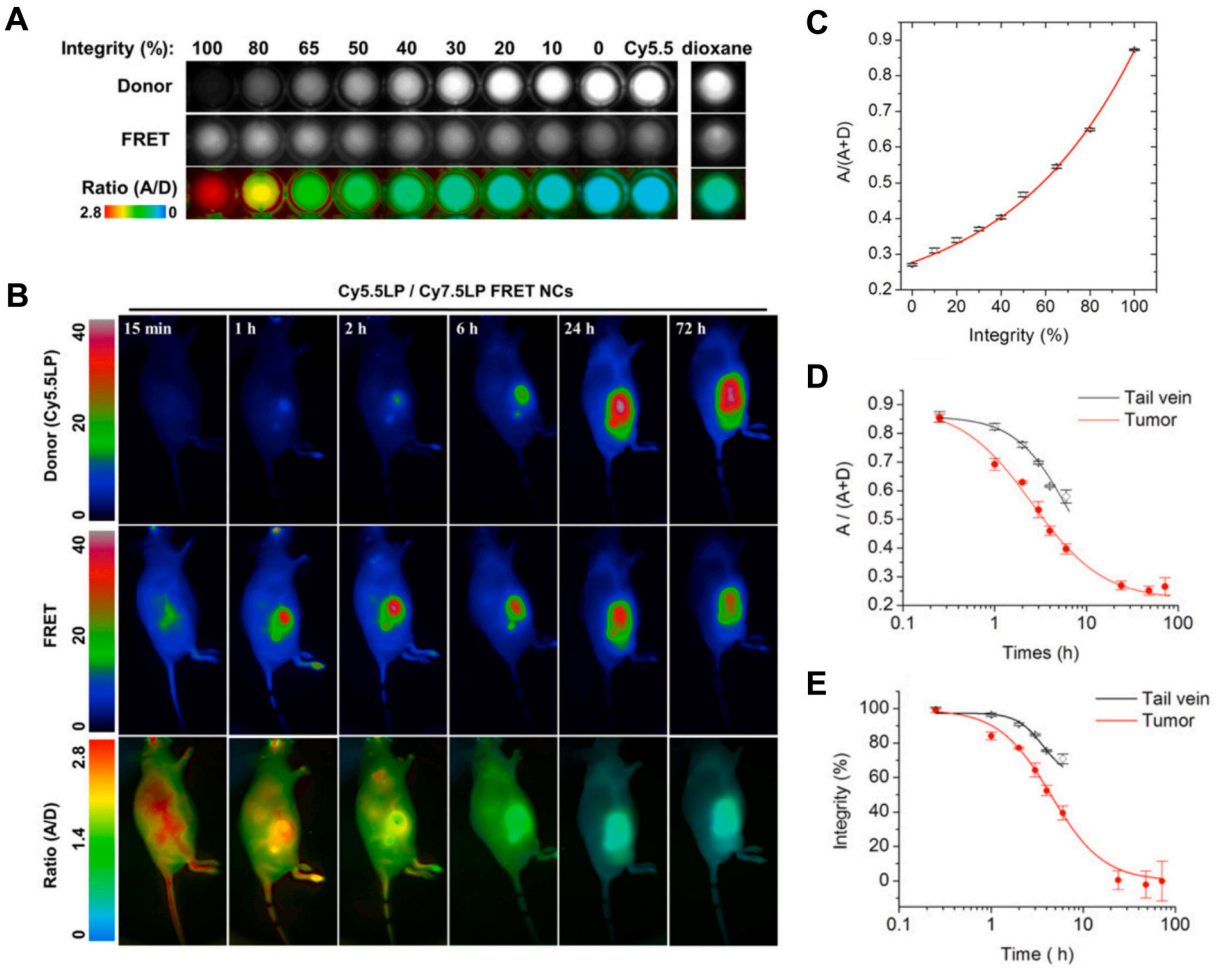


Fig. 13. An example of a semi-quantitative FRET assay in a tumor-bearing mouse model using IVIS, by Bouchaala et al. [57]. LNEs were analyzed on the *in vivo* particle stability and biodistribution. A) and C) The calibration curves between proximity ratio (PR), % integrity, and pseudocolors for the conversion of the FRET signal to %integrity. B) The IVIS image of the rats injected with FRET-LNEs over 72 h; the last row shows the PR being converted to pseudocolors of the particle integrity overlaying the tumor-bearing mouse images. D) The proximity ratio information obtained from the tail vein and tumor area expressed as a function of time and then converted to E) % integrity by the calibration curve in graph C). Adapted from [57]. Copyright 2016, Elsevier under a Creative Commons CC-BY license.

4.2.2.2. Nanospheres. Later, Cayre et al. [38] demonstrated the application of a semi-quantitative FRET assay for the particle stability of squalene-gemcitabine bioconjugate nanoparticles (SQGem) in mouse liver. A pair of FRET dyes, Cy5.5 (donor) and Cy7.5 (acceptor), were conjugated to squalene moiety turning into squalene-Cy5.5 (SQCy5.5) and squalene-Cy7.5 (SQCy7.5). Then SQGem, SQCy5.5, and SQCy7.5 were all mixed and put to precipitate to form FRET-SQGem nanoparticles. The nanoparticles were intravenously injected into mice, and the fluorescence images around the liver area were taken using the IVIS. The fluorescent intensity was converted to the numerical value using Living Image software (PerkinElmer). Then, the FRET proximity ratio was calculated to determine the particle integrity. With this method, the authors hypothesized that the FRET proximity ratio could be correlated to the proportion of intact FRET-SQGem nanoparticles and dissociated FRET-SQGem remnants (separated SQCy5.5 and SQCy7.5 moieties) accumulating in fatty tissues of the liver. Therefore, the proximity ratio could be converted to the relative percentage of the intact FRET-SQGem, called %integrity, *via* the calibration curve. The %integrity calibration curve was constructed by mixing the fully intact FRET-SQGem nanoparticles with various percentages of the nanoparticles purely made of the SQCy5.5 or SQCy7.5. The proximity ratio closing to 1.0 was converted to 100% of intact nanoparticles, and a decrease in the proximity ratio meant a decrease in the population of the intact nanoparticle and loss of particle stability. The image from IVIS around the mouse's liver area revealed for the first time that intact FRET-SQGem could be observed in the liver for 56% at 35 min after the injection and then dropped to lower than 10% after 2 h, indicating the dissociation of SQGem in the liver with no persistent accumulation, which is desirable for reducing liver toxicity. This FRET system allowed for the semi-quantitative assay of intact FRET-SQGem in the mouse's liver with the advantage that this technique is non-invasive and can be performed in live animals. The author suggested that the method could be used for a future study on the biodistribution of SQGem in other areas of the rat body. However, this FRET system still had low signal penetration (<1 cm), and the new FRET system with the emission in the NIR-II region (1000–1700 nm) may need to be developed for a future experiment.

4.2.3. FRET-IVIS for oral nanomedicine

4.2.3.1. Nanospheres. EGTA-conjugated nanoparticles are the polymeric-based nanoparticles developed by Chuang et al. [50,51] to deliver insulin *via* the oral route. It is a pH-responsive nanoparticle consisting of chitosan and poly-(γ-glutamic acid) conjugated with ethylene glycol tetra-acetic acid (CS/γPGA-EGTA) in which insulin can be loaded. The nanoparticles themselves can facilitate paracellular absorption of insulin as well as protect the insulin from gastrointestinal enzymes. Therefore, to test the protective effect of the γPGA-EGTA nanoparticles, insulin stability was investigated in rats by comparing the naked insulin and the insulin with γPGA-EGTA nanoparticles. FRET was used for the semi-quantitative assay of insulin stability relating to the protective effect of γPGA-EGTA nanoparticles. The FRET donor and acceptor were conjugated to insulin on the opposite end of the amino chain before being loaded into the nanoparticles (Fig. 4C). Rat's duodenum was cut open and tied up to make a closed loop. Then, the FRET-insulin-loading nanoparticles and naked FRET-insulin were directly injected into the lumen of the said loop. After specific time points, live FRET imagery of the duodenum loop was taken over time using IVIS. FRET acceptor intensity signal was quantified by the software with their maximum values normalized to 100%. The amount of stable FRET-insulin was semi-quantitatively estimated. The comparison between the amount of the naked FRET-insulin and the loading insulin allowed for the protective effect of the γPGA-EGTA nanoparticles to be determined. The results found that, in 2 h, the % normalized acceptor intensity of naked insulin plummeted to 40%, while the encapsulated insulin remained at 80%, meaning that γPGA-EGTA nanoparticles had a good protective effect for insulin against the intestinal enzyme. Besides, the nanoparticle also increased the oral bioavailability of insulin to 18% when compared to 0.1% by the orally given free-form insulin powder. The orally given nano-encapsulated insulin significantly reduced plasma glucose during the oral glucose tolerance test compared to the control group. This research is the most unique among all since FRET is implemented to study the stability of the encapsulated insulin rather than the integrity of the nanoparticles.

4.2.3.2. Liposomes. Semi-quantitative and qualitative FRET application in the *in vivo* oral absorption study of the liposomes (LPs) with various sizes (conventional LPs at 100, 200, 500 nm) and surface modifications (conventional, anionic, cationic, PEGylated LPs at 200 nm) were also developed by Liu et al. [48]. Similar to the nanocapsules, carbocyanine dyes could be directly co-encapsulated inside the LPs voids making the FRET-LPs. The semi-quantitative FRET technique was developed at first and employed in the *in vitro* particle stability experiment, in which FRET-LPs were incubated in various gastrointestinal fluids. FRET acceptor signal could be retrieved by using the IVIS. With the quantification software, the FRET intensity was converted to the % total radiant efficiency, which is then normalized to the percentage implying the number of intact LPs. Thereafter, the same technique could be utilized for the study of the *in vivo* particle stability in the gastrointestinal (GI) tract and biodistribution. Firstly, mice were orally given the FRET-LPs and then sacrificed at several time points with their GI tract and internal organs harvested. Then, IVIS was utilized with the whole *ex vivo* GI tract image taken, and the FRET intensity was quantified into the % total radiant efficiency. Thus, the percentage amount of intact FRET-LPs over 4 h in each part of the GI tract (stomach, duodenum, jejunum, *etc.*) and other intestinal organs could be estimated. The result indicated that smaller size conventional LPs, (200 nm) cationic LPs, and (200 nm) PEGylated LPs were more stable as they could be retained longer in the GI tract. Besides, no fluorescence signals were found in the *ex vivo* internal organs meaning that the intact LPs did not absorb into the circulatory system. Further study on the oral bioavailability of doxorubicin-encapsulated LPs also had the exact correlation. It confirmed that better particle stability and longer GI retention of the small-sized LPs, the cationic LPs, and the PEGylated LPs resulted in the increase in oral bioavailability of doxorubicin, despite no intact LPs found in the circulatory system. This article demonstrates that the semi-quantitative FRET technique could help to elucidate the association between the LPs particle integrity and the increase in oral bioavailability of the encapsulated drug, by which it could pave the way to a better LP design in the future.

4.3. FRET fluorometry of blood and plasma

For the small liquid *in vitro* samples such as blood, plasma, and small tissue, a microplate reader or a fluorometer are adequate for obtaining the fluorescence spectrum and the intensity values of FRET.

4.3.1. Micelles

Semi-quantitative FRET fluorimetry was developed to investigate and compare the *in vivo* particle stability and plasma particle concentration of the ordinary non-cross-linked PEG^{5k}-CA_8 micelles (NCMN) and the disulfide cross-linked PEG^{5k}-Cys_4-CA_8 micelles (DCMN) [54]. The FRET-NCMN and FRET-DCMN were injected intravenously into nude mice with blood collected over time. The samples were then analyzed for FRET by the microplate reader. The FRET proximity ratio (PR) was calculated and normalized to the percentage (called % FRET ratio), allowing for the semi-quantitative assay of the relative plasma particle concentration (Fig. 14). The result showed that FRET-DCMN was more stable over 24 h in blood than the FRET-NCMN. Further FRET *in vitro* assay was able to evidence that lipoproteins caused the rapid dissociation of FRET-NCMN.

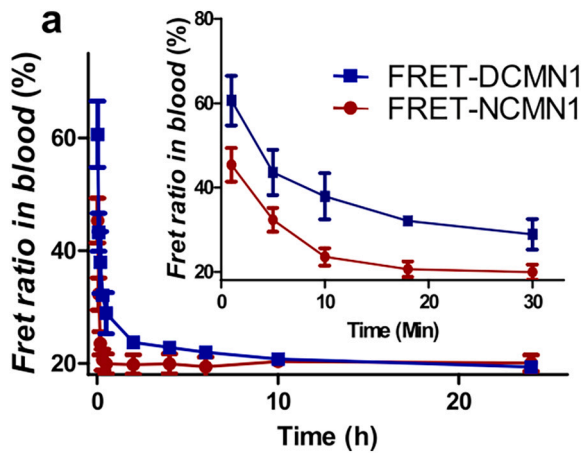


Fig. 14. An example of semi-quantitative FRET fluorometry for particle concentration assay in a mouse model using microplate reader, by Li et al. [54]. Telodendrimers nanoparticles (DCMN and NCMN) were analyzed for the *in vivo* plasma particle concertation. The PR was obtained from mouse blood and then normalized as a relative percentage (called % FRET ratio in the article). Reprinted with permission from [54], Copyright 2012 American Chemical Society.

Zhang et al. [47] also performed the semi-quantitative assay for analyzing the plasma particle concentration of PEG-PCL micelles. The FRET-micelles were intravenously injected into mice with blood collected over time. The plasma was then extracted, and the sample was analyzed by the fluorimeter. The intensity was converted to the % integrity *via* the calibration curve developed specifically for this FRET system. Similar to the technique of Cayre et al. [38] in the SQGem nanoparticles, the calibration curve was built by mixing various concentrations of the co-conjugated FRET micelles (with NBD-X and MS735 together) with the mixture of NBD-X micelles and MS735 micelles. The co-conjugated FRET-micelles represent the percentage of the intact micelles, while the mixture of NBD-X micelles and MS735 micelles simulate the signals of the dissociated FRET remnants. The % integrity was considered as a semi-quantitative parameter since it provided only the relative percentage, not the true particle numbers. The % integrity of the micelles in plasma declined gradually and reached 60% after 72 h. The study successfully demonstrated the new FRET pair and the semi-quantitative FRET technique for determining the plasma particle concentration of the micelles in mice.

4.3.2. Nanocrystals

Zhang et al. [53] also utilized semi-quantitative FRET fluorimetry to determine the plasma particle concentration of FRET-curcumin nanocrystals. Mice were intravenously injected with the FRET-curcumin nanocrystal, and the blood was collected for up to 24 h. The plasma was extracted from the blood sample thereafter and then analyzed for FRET using the microplate reader. The FRET signal was recorded at 635 nm and converted to the concentration of the FRET-curcumin nanocrystal expressed in mass concentration (ng/μL). The curcumin nanocrystals were found in plasma for up to 4 h after a single-dose intravenous injection (15 mg/kg). However, neither the FRET excitation wavelength nor the quantification calibration curve was elaborated.

4.3.3. Nanospheres

c(CRGDKGPDC) peptide (iRGD) modified hyaluronic acid–deoxycholic acid conjugate (iRGD-PEG-HA-DOCA, IPHD) is a self-assembly polymeric nanosphere developed by Liu et al. [49] to deliver dasatinib to a solid tumor. Dasatinib and FRET pair dyes were loaded together into the nanoparticles' matrix allowing for the semi-quantitative FRET assay of the plasma particle concentration and *in vivo* particle integrity. The nanoparticles were also further biomineralized by calcium phosphate, called $Ca_3(PO_4)_2$-iRGD-PEG-HA-DOCA (CIPHD), by coating with calcium phosphate, aiming for the pH-responsive property. The FRET-IPHD/Dasatinib and the FRET-CIPHD/Dasatinib were injected into rats, and blood samples were collected after several time points. The plasma was separated from the sample and then analyzed for FRET by the fluorometer. FRET proximity ratio (called FRET ratio in the article) was calculated and normalized to a percentage. This value was interpreted as the relative percentage of the nanoparticle's plasma concentration, inferring the *in vivo* particle integrity of the FRET-IPHD and FRET-CIPHD.

These FRET experiments aimed at proving whether biomineralization increases particle stability or not. The result found that the non-mineralized FRET-IPHD/Dasatinib was less stable than the mineralized FRET-CIPHD in the rat's blood circulation. The normalized PR of FRET-CIPDH/Dasatinib in blood stayed at around 60% up to 24 h, while the normalized PR value from FRET-IPDH/Dasatinib dropped from 77% to 50% just in 30 min. The higher blood particle stability of CIPHD/Dasatinib also resulted in a higher AUC and half-life of plasma dasatinib (analyzed by HPLC, thus indistinguishable between the free drug or the encapsulated drugs). This also resonated with the *in vivo* result of CIPDH/Dasatinib having higher efficacy than IPDH/Dasatinib to increase the survival of tumor-bearing mice. This article is an example that the FRET semi-quantitative assay helped to prove that higher particle stability due to biomineralization (not by other processes) contributed to a better anti-tumor efficacy for this type of nanoparticle.

5. Conclusion

Currently, most of the FRET *in vivo* nanoparticle tracking techniques are the qualitative imagery and the semi-quantitative assay on *in vivo* particle stability, biodistribution, cargo release, and plasma particle concentration. Some unique techniques were also developed, such as the FRET study on the protective effect of the nanoparticle against the intestinal enzyme on insulin [50,51], oral absorption [48], and the reversed FRET for determining the cargo release [44]. It is clear that FRET is still mainly employed for *in vivo* particle stability and biodistribution study. There are only two *in vivo* FRET studies on oral absorption and none from other absorption routes nor the excretion pathway. It is also obvious that there is a lack of quantitative assay, which also leads to the lack of advanced pharmacokinetics of the nanoparticles.

Different instruments were used for the FRET assay, namely CFM, IVIS, fluorometer, and microplate reader. All the instruments are capable of performing the semi-quantitative assay, while only CFM and IVIS can perform qualitative and semi-quantitative imaging analysis. IVIS has the advantages of being a non-invasive technique and having high flexibility to analyze various kinds of samples ranging from a well-plate, *ex vivo* organs, and live full-body imagery. It turns out that the spatial resolution of IVIS is rather low due to high signal interference and low tissue penetration. Therefore, for the biodistribution study, only large organs such as the liver can give a relatively high resolution for FRET whole-body live imaging. For other smaller organs, it really needs validation and correlation from the invasive *ex vivo* organs imaging or other techniques such as CFM. Besides, IVIS also requires complex signal calibration procedures such as the pseudocolors technique in order to be semi-quantitative. These hurdles make it difficult to obtain the true quantitative assay on particle numbers to be obtained from IVIS. However, IVIS is still the popular instrument of choice as being mostly employed in much recent literature, possibly due to its versatility and benefits in giving both live imagery and semi-quantitative % intact nanoparticles. In addition, CFM is less flexible for the use than IVIS. It was mainly used for analyzing the *ex vivo* tissue samples or a very small animal model like zebrafish larva [43,52]. The zebrafish larva as an animal model is adapted for quickly demonstrating the FRET system as the larva is transparent and tiny, but one must take into consideration that the evidence for the clinical translation of this animal model in

terms of pharmacokinetics is still extremely limited. A rodent model is still preferential as it has more solid evidence to support its pharmacokinetics translation to humans [58,59] and is also considered a goal standard in the preclinical stage [60]. Besides, CFM is also utilized for live FRET imaging on the mouse's earlobe vasculature [41,42]. This earlobe technique was one of the earliest to be developed using FRET, but it is limited only to micelles and was overshadowed by the development of IVIS. Moreover, the FRET fluorimetry is used only for analyzing blood samples to obtain the semi-quantitative plasma particle concentration, as the fluorimeter is not an imaging instrument. Despite being very specific to the plasma particle concentration, this technique has the highest potentiality to be developed into a true quantitative assay, which requires the construction of a proper calibration curve to link the intensity value or FRET proximity ratio to the particle number. However, due to the fact that the technique involves extracting nanoparticles from plasma, an extraction method that can ensure the stability of nanoparticles during the process needs to be implemented.

To conclude, true quantitative *in vivo* tracking of nanomedicine is important. Without the information on the intact nanoparticle number in plasma and organs, it is not possible to perform any advanced pharmacokinetics such as the physiologically based pharmacokinetic modeling (PBPK). Thus, this is one of the reasons for the lack of pharmacokinetic models on the nanomedicine [8], causing a problem in the translation to the clinical trial. Despite its necessity, there is a lack of quantitative assay for nanomedicine, even for the *in vitro* experiments, as researchers still focus on the pharmacokinetics of the encapsulated drugs, ignoring the fact that the nanocarriers also have their own fate that can greatly affect the drug efficacy. In brief, FRET is an effective tool for *in vivo* tracking the nanomedicine to investigate the pharmacokinetics of nanomedicine, especially the *in vivo* particle stability and biodistribution. However, it still has a limitation for not reaching the level of true quantitative assay yet. And as such, the advanced pharmacokinetic analysis could not be completely achieved.

Declaration of Competing Interest

The authors declare that they have no known competing financial interests or personal relationships that could have appeared to influence the work reported in this paper.

Acknowledgements

This work was supported by the Ligue Contre le Cancer, Maine-et-Loire Committee (49), Angers, France (#JPB/FP – 223/12.2020).

References

[1] B. Flühmann, I. Ntai, G. Borchard, S. Simoens, S. Mühlebach, Nanomedicines: the magic bullets reaching their target? Eur. J. Pharm. Sci. 128 (2019) 73–80, https://doi.org/10.1016/j.ejps.2018.11.019.
[2] F. Farjadian, A. Ghasemi, O. Gohari, A. Roointan, M. Karimi, M.R. Hamblin, Nanopharmaceuticals and nanomedicines currently on the market: Challenges and opportunities, 2019, https://doi.org/10.2217/nnm-2018-0120.
[3] M.J. Mitchell, M.M. Billingsley, R.M. Haley, M.E. Wechsler, N.A. Peppas, R. Langer, Engineering precision nanoparticles for drug delivery, Nat. Rev. Drug Discov. 20 (2021) 101–124, https://doi.org/10.1038/s41573-020-0090-8.
[4] K. Greish, A. Mathur, M. Bakhiet, S. Taurin, Nanomedicine: is it lost in translation? Ther. Deliv. 9 (2018) 269–285, https://doi.org/10.4155/tde-2017-0118.
[5] H.L. Jang, Y.S. Zhang, A. Khademhosseini, Boosting clinical translation of nanomedicine, Nanomedicine 11 (2016) 1495–1497, https://doi.org/10.2217/nnm-2016-0133.
[6] D. Sun, S. Zhou, W. Gao, What went wrong with anticancer nanomedicine design and how to make it right, ACS Nano 14 (2020) 12281–12290, https://doi.org/10.1021/acsnano.9b09713.
[7] V. Agrahari, V. Agrahari, Facilitating the translation of nanomedicines to a clinical product: challenges and opportunities, Drug Discov. Today 23 (2018) 974–991, https://doi.org/10.1016/j.drudis.2018.01.047.
[8] V. Lebreton, S. Legeay, P. Saulnier, F. Lagarce, Specificity of pharmacokinetic modeling of nanomedicines, Drug Discov. Today 26 (2021) 2259–2268, https://doi.org/10.1016/j.drudis.2021.04.017.
[9] S. Bonnet, R. Elfatairi, F. Franconi, E. Roger, S. Legeay, Organic nanoparticle tracking during pharmacokinetic studies, Nanomedicine 16 (2021), https://doi.org/10.2217/nnm-2021-0155, 2539–2536.
[10] M. Germain, F. Caputo, S. Metcalfe, G. Tosi, K. Spring, A.K.O. Åslund, A. Pottier, R. Schiffelers, A. Ceccaldi, R. Schmid, Delivering the power of nanomedicine to patients today, J. Control. Release 326 (2020) 164–171, https://doi.org/10.1016/j.jconrel.2020.07.007.
[11] C. Pérez-Medina, A.J.P. Teunissen, E. Kluza, W.J.M. Mulder, R. van der Meel, Nuclear imaging approaches facilitating nanomedicine translation, Adv. Drug Deliv. Rev. 154–155 (2020) 123–141, https://doi.org/10.1016/j.addr.2020.07.017.
[12] Marcin Ptaszek, Chapter three – rational design of fluorophores for in vivo applications, in: M.C. Morris (Ed.), Fluorescence-Based Biosensors, Academic Press, 2013, pp. 59–108, https://doi.org/10.1016/B978-0-12-386932-6.00003-X.
[13] T. Etrych, O. Janoušková, P. Chytil, Fluorescence imaging as a tool in preclinical evaluation of polymer-based nano-DDS systems intended for cancer treatment, Pharmaceutics. 11 (2019), https://doi.org/10.3390/pharmaceutics11090471.
[14] D.M. Charron, G. Zheng, Nanomedicine development guided by FRET imaging, Nano Today 18 (2018) 124–136, https://doi.org/10.1016/j.nantod.2017.12.006.
[15] T. Chen, B. He, J. Tao, Y. He, H. Deng, X. Wang, Y. Zheng, Application of Förster Resonance Energy Transfer (FRET) technique to elucidate intracellular and in vivo biofate of nanomedicines, Adv. Drug Deliv. Rev. 143 (2019) 177–205, https://doi.org/10.1016/j.addr.2019.04.009.
[16] H. Sahoo, Förster resonance energy transfer - a spectroscopic nanoruler: principle and applications, J. Photochem. Photobiol. C: Photochem. Rev. 12 (2011) 20–30, https://doi.org/10.1016/j.jphotochemrev.2011.05.001.
[17] A.S. Klymchenko, F. Liu, M. Collot, N. Anton, Dye-loaded nanoemulsions: biomimetic fluorescent Nanocarriers for bioimaging and nanomedicine, Adv. Healthcare Mater. 10 (2021) 1–27, https://doi.org/10.1002/adhm.202001289.
[18] T. Förster, Energy migration and fluorescence, J. Biomed. Opt. 17 (2012), 011002, https://doi.org/10.1117/1.jbo.17.1.011002.
[19] R.M. Clegg, The history of FRET: from conception through the labors of birth, Rev. Fluoresc. 3 (2006) 1–45.
[20] B.W. van der Meer, Förster Theory, in: FRET – Förster Resonance Energy Transfer, John Wiley & Sons, Ltd, 2013, pp. 23–62, https://doi.org/10.1002/9783527656028.ch03.
[21] A. Kaur, P. Kaur, S. Ahuja, Förster resonance energy transfer (FRET) and applications thereof, Anal. Methods 12 (2020) 5532–5550, https://doi.org/10.1039/D0AY01961E.
[22] N. Hildebrandt, How to apply FRET: from experimental design to data analysis, in: FRET – Förster Resonance Energy Transfer, John Wiley & Sons, Ltd, 2013, pp. 105–163, https://doi.org/10.1002/9783527656028.ch05.
[23] J.R. Lakowicz, Energy transfer, in: Principles of Fluorescence Spectroscopy, Springer US, Boston, MA, 2006, pp. 443–475, https://doi.org/10.1007/978-0-387-46312-4_13.
[24] M. Dahan, A.A. Deniz, T. Ha, D.S. Chemla, P.G. Schultz, S. Weiss, Ratiometric measurement and identification of single diffusing molecules, Chem. Phys. 247 (1999) 85–106.
[25] B. Wallace, P.J. Atzberger, Förster resonance energy transfer: role of diffusion of fluorophore orientation and separation in observed shifts of FRET efficiency, PLoS One (2017) 1–22, https://doi.org/10.1371/journal.pone.0177122 May.
[26] E. Nir, X. Michalet, K.M. Hamadani, T.A. Laurence, D. Neuhauser, Shot-noise limited single-molecule FRET histograms: comparison between theory and experiments, J. Phys. Chem. B 110 (2006) 22103–22124, https://doi.org/10.1021/jp063483n.
[27] J.J. Mccann, U.B. Choi, L. Zheng, K. Weninger, M.E. Bowen, Optimizing methods to recover absolute FRET efficiency from immobilized single molecules, Biophys. J. 99 (2010) 961–970, https://doi.org/10.1016/j.bpj.2010.04.063.
[28] J.P. Torella, S.J. Holden, Y. Santoso, J. Hohlbein, A.N. Kapanidis, Identifying molecular dynamics in single-molecule FRET experiments with burst variance analysis, Biophys. J. 100 (2011) 1568–1577, https://doi.org/10.1016/j.bpj.2011.01.066.
[29] J. Gravier, L. Sancey, S. Hirsjärvi, E. Rustique, C. Passirani, J.P. Benoît, J.L. Coll, I. Texier, FRET imaging approaches for in vitro and in vivo characterization of synthetic lipid nanoparticles, Mol. Pharm. 11 (2014) 3133–3144, https://doi.org/10.1021/mp500329z.
[30] X. Guo, F. Liu, J. Deng, P. Dai, Y. Qin, Z. Li, B. Wang, A. Fan, Z. Wang, Y. Zhao, Electron-accepting micelles deplete reduced nicotinamide adenine dinucleotide phosphate and impair two antioxidant cascades for ferroptosis-induced tumor eradication, ACS Nano 14 (2020) 14715–14730, https://doi.org/10.1021/acsnano.0c00764.
[31] P.J. Robinson, C.A. Woolhead, Implementation of FRET technologies for studying the folding and conformational changes in biological structures, in: FRET – Förster Resonance Energy Transfer, John Wiley & Sons, Ltd, 2013, pp. 357–396, https://doi.org/10.1002/9783527656028.ch09.
[32] K. Suhling, L.M. Hirvonen, J.A. Levitt, P.-H. Chung, C. Tregidgo, A. le Marois, D. A. Rusakov, K. Zheng, S. Ameer-Beg, S. Poland, S. Coelho, R. Henderson, N. Krstajic, Fluorescence lifetime imaging (FLIM): basic concepts and some recent developments, Med. Photon. 27 (2015) 3–40, https://doi.org/10.1016/j.medpho.2014.12.001.
[33] R. Datta, T.M. Heaster, J.T. Sharick, A.A. Gillette, M.C. Skala, Fluorescence lifetime imaging microscopy: fundamentals and advances in instrumentation, analysis, and applications, J. Biomed. Opt. 25 (2020) 1–43, https://doi.org/10.1117/1.JBO.25.7.071203.
[34] Thermo Fisher Scientific, Fluorescent tracers derivatives of cell morphology and fluid flow, in: The Molecular Probes Handbook, 2010, pp. 588–648.

[35] National Center for Biotechnology Information, PubChem Compound Summary for CID 126455658, Cy3 Carboxylic acids, (n.d.). https://pubchem.ncbi.nlm.nih.gov/compound/Cy3-Carboxylic-acids (accessed March 4, 2022).
[36] National Center for Biotechnology Information, PubChem Compound Summary for CID 86276410, Cy5 Carboxylic acids, (n.d.). https://pubchem.ncbi.nlm.nih.gov/compound/Cy5-Carboxylic-acids (accessed March 4, 2022).
[37] National Center for Biotechnology Information, PubChem Compound Summary for CID 91757848, Cy7-carboxylic acid chloride, (n.d.). https://pubchem.ncbi.nlm.nih.gov/compound/Cy7-carboxylic-acid-chloride (accessed March 4, 2022).
[38] F. Cayre, S. Mura, B. Andreiuk, D. Sobot, S. Gouazou, D. Desmaële, A. S. Klymchenko, P. Couvreur, In vivo FRET imaging to predict the risk associated with hepatic accumulation of squalene-based prodrug nanoparticles, Adv. Healthc. Mater. 7 (2018), https://doi.org/10.1002/adhm.201700830.
[39] National Center for Biotechnology Information, PubChem Compound Summary for CID 5282412, Indocyanine green, (n.d.). https://pubchem.ncbi.nlm.nih.gov/compound/Indocyanine-green (accessed March 4, 2022).
[40] H. Chen, S. Kim, W. He, H. Wang, P.S. Low, K. Park, J.X. Cheng, Fast release of lipophilic agents from circulating PEG-PDLLA micelles revealed by in vivo Förster resonance energy transfer imaging, Langmuir. 24 (2008) 5213–5217, https://doi.org/10.1021/la703570m.
[41] S.Y. Lee, S. Kim, J.Y. Tyler, K. Park, J.X. Cheng, Blood-stable, tumor-adaptable disulfide bonded mPEG-(Cys)4-PDLLA micelles for chemotherapy, Biomaterials. 34 (2013) 552–561, https://doi.org/10.1016/j.biomaterials.2012.09.065.
[42] K. Ishizawa, K. Togami, H. Tada, S. Chono, Multiscale live imaging using Förster Resonance Energy Transfer (FRET) for evaluating the biological behavior of nanoparticles as drug carriers, J. Pharm. Sci. 109 (2020) 3608–3616, https://doi.org/10.1016/j.xphs.2020.08.028.
[43] J. Tao, Z. Wei, Y. He, X. Yan, S. Ming-Yuen Lee, X. Wang, W. Ge, Y. Zheng, Toward understanding the prolonged circulation and elimination mechanism of crosslinked polymeric micelles in zebrafish model, Biomaterials. 256 (2020) 1–17, https://doi.org/10.1016/j.biomaterials.2020.120180.
[44] P. Zou, H. Chen, H.J. Paholak, D. Sun, Noninvasive fluorescence resonance energy transfer imaging of in vivo premature drug release from polymeric nanoparticles, Mol. Pharm. 10 (2013) 4185–4194, https://doi.org/10.1021/mp4002393.
[45] M.A. Quadir, S.W. Morton, Z.J. Deng, K.E. Shopsowitz, R.P. Murphy, T.H. Epps, P. T. Hammond, PEG-polypeptide block copolymers as pH-responsive endosome-solubilizing drug nanocarriers, Mol. Pharm. 11 (2014) 2420–2430, https://doi.org/10.1021/mp500162w.
[46] S.W. Morton, X. Zhao, M.A. Quadir, P.T. Hammond, FRET-enabled biological characterization of polymeric micelles, Biomaterials. 35 (2014) 3489–3496, https://doi.org/10.1016/j.biomaterials.2014.01.027.
[47] H. Zhang, H. Li, Z. Cao, J. Du, L. Yan, J. Wang, Investigation of the in vivo integrity of polymeric micelles via large stokes shift fluorophore-based FRET, J. Control. Release 324 (2020) 47–54, https://doi.org/10.1016/j.jconrel.2020.04.046.
[48] W. Liu, D. Li, Z. Dong, K. Liu, H. He, Y. Lu, W. Wu, Q. Li, L. Gan, J. Qi, Insight into the in vivo translocation of oral liposomes by fluorescence resonance energy transfer effect, Int. J. Pharm. 587 (2020), https://doi.org/10.1016/j.ijpharm.2020.119682.
[49] Y. Liu, L. Li, J. Liu, M. Yang, H. Wang, X. Chu, J. Zhou, M. Huo, T. Yin, Biomineralization-inspired dasatinib nanodrug with sequential infiltration for effective solid tumor treatment, Biomaterials. 267 (2021), 120481, https://doi.org/10.1016/j.biomaterials.2020.120481.
[50] E.Y. Chuang, K.J. Lin, F.Y. Su, F.L. Mi, B. Maiti, C.T. Chen, S.P. Wey, T.C. Yen, J. H. Juang, H.W. Sung, Noninvasive imaging oral absorption of insulin delivered by nanoparticles and its stimulated glucose utilization in controlling postprandial hyperglycemia during OGTT in diabetic rats, J. Control. Release 172 (2013) 513–522, https://doi.org/10.1016/j.jconrel.2013.05.006.
[51] E.-Y. Chuang, K.-J. Lin, F.-Y. Su, H.-L. Chen, B. Maiti, Y.-C. Ho, T.-C. Yen, N. Panda, H.-W. Sung, Calcium depletion-mediated protease inhibition and apical-junctional-complex disassembly via an EGTA-conjugated carrier for oral insulin delivery, J. Control. Release 169 (2013) 296–305, https://doi.org/10.1016/j.jconrel.2012.11.011.
[52] Y. Li, X. Miao, T. Chen, X. Yi, R. Wang, H. Zhao, S.M.Y. Lee, X. Wang, Y. Zheng, Zebrafish as a visual and dynamic model to study the transport of nanosized drug delivery systems across the biological barriers, Colloids Surf. B: Biointerfaces 156 (2017) 227–235, https://doi.org/10.1016/j.colsurfb.2017.05.022.
[53] J. Zhang, Y.C. Liang, X. Lin, X. Zhu, L. Yan, S. Li, X. Yang, G. Zhu, A.L. Rogach, P.K. N. Yu, P. Shi, L.C. Tu, C.C. Chang, X. Zhang, X. Chen, W. Zhang, C.S. Lee, Self-monitoring and self-delivery of photosensitizer-doped nanoparticles for highly effective combination cancer therapy in vitro and in vivo, ACS Nano 9 (2015) 9741–9756, https://doi.org/10.1021/acsnano.5b02513.
[54] Y. Li, M.S. Budamagunta, J. Luo, W. Xiao, J.C. Voss, K.S. Lam, Probing of the assembly structure and dynamics within nanoparticles during interaction with blood proteins, ACS Nano 6 (2012) 9485–9495, https://doi.org/10.1021/nn302317j.
[55] Y. Tang, X. Wang, J. Li, Y. Nie, G. Liao, Y. Yu, C. Li, Overcoming the reticuloendothelial system barrier to drug delivery with a "don't-Eat-Us" strategy, ACS Nano (2019), https://doi.org/10.1021/acsnano.9b05679.
[56] A.L. Lainé, J. Gravier, M. Henry, L. Sancey, J. Béjaud, E. Pancani, M. Wiber, I. Texier, J.L. Coll, J.P. Benoit, C. Passirani, Conventional versus stealth lipid nanoparticles: formulation and in vivo fate prediction through FRET monitoring, J. Control. Release 188 (2014) 1–8, https://doi.org/10.1016/j.jconrel.2014.05.042.
[57] R. Bouchaala, L. Mercier, B. Andreiuk, Y. Mély, T. Vandamme, N. Anton, J. G. Goetz, A.S. Klymchenko, Integrity of lipid nanocarriers in bloodstream and tumor quantified by near-infrared ratiometric FRET imaging in living mice, J. Control. Release 236 (2016) 57–67, https://doi.org/10.1016/j.jconrel.2016.06.027.
[58] C.H.C. Leenaars, C. Kouwenaar, F.R. Stafleu, A. Bleich, M. Ritskes-Hoitinga, R.B. M. de Vries, F.L.B. Meijboom, Animal to human translation: a systematic scoping review of reported concordance rates, J. Transl. Med. 17 (2019) 1–22, https://doi.org/10.1186/s12967-019-1976-2.
[59] T. Denayer, T. Stöhrn, M. van Roy, Animal models in translational medicine: validation and prediction, New Horiz. Transl. Med. 2 (2014) 5–11, https://doi.org/10.1016/j.nhtm.2014.08.001.
[60] M.S. Valic, M. Halim, P. Schimmer, G. Zheng, Guidelines for the experimental design of pharmacokinetic studies with nanomaterials in preclinical animal models, J. Control. Release 323 (2020) 83–101, https://doi.org/10.1016/j.jconrel.2020.04.002.

View publication stats